LAPIN AMK
Lapland University of Applied Sciences

Laser assisted post-weld cleaning of austenitic stainless steels.

especially about pitting corrosion

Ehrenbrandtner Antonia Maria

Thesis

Double Degree
Bachelor

2023

LAPIN AMK
Lapland University of Applied Sciences

Bachelor thesis
Laser assisted post-weld cleaning of
austenitic stainless steels

Author(s)	Antonia Ehrenbrandtner	**Year**	2023
Supervisor(s)	Timo Kauppi		
Title	Laser Assisted Post-Weld Cleaning of Stainless Steels.		
Number of pages	84 + 4		

In this work, the cleaning of welds by laser and its effects on the corrosion resistance of austenitic stainless steel were analysed. The oxide layer was removed from the welded samples with different settings of the laser. By means of six different experiments, a concise statement could be made as to the influence of the different settings.

The following methods were used for the experiments: "Salt spray", "ASTM G61-86", "EDS-analysis", "Standardized effects", "Light microscope" and "ASTM G48-11". After three test runs, it was possible to determine which laser parameters have the most influence on corrosion resistance. In particular, how the laser cleaning changed the material surface and its elements.

The best results were compared with two other papers, where the weld was cleaned conventionally. Conventional means that the samples were cleaned chemically or electrochemically. It is clear that the oxidation layer with laser ablation is a very good and environmentally friendly alternative.

Keywords	post- weld cleaning, laser cleaning, pitting corrosion, chemical cleaning,
Special remarks	Cooperation with the company "Cajo technologies" to remove the oxidation layer formed after welding with a laser.

FOREWORD

Thank you so much for the great dedication you have always shown to me. Without such a loving, funny, and cheerful professor, this great bachelor thesis would never have been possible. It is truly unimaginable how many hours you invested in this work for me for months on end, and I am very grateful for that. Thank you for driving me to and from the company and for being able to solve any problem, no matter how small, in a minute. You never lost your joy for work, and my interest in metallurgy only continued to grow. Timo Kauppi, I will always be infinitely grateful to you for the wonderful time that I was able to spend with you. Thank you very much for that!

Without the technical genius trio of Jouni Kanto, Markus Harrinkoski, and Jussi Suopajärvi, this bachelor thesis would not have been possible. Thank you for spending hours and months showing me how to weld properly and how to use the plasma cutter. When something was too heavy, you were able to carry it effortlessly. Even when you were very stressed yourselves, you always managed to have time for me. Thank you.

Thanks to Soile, it was possible to get every machine working and make the necessary adjustments. With her expertise, she was always able to help me, and when it still did not work, she listened and encouraged me.

The provision of the laser machine from the company "Cajo Technologies" made this bachelor thesis possible. Many thanks to Niko Karsikas and Tom Karsikas for introducing me to the machine.

Many thanks for providing the sample material from the company "Outokumpu," especially Mr. Hannu-Pekka Heikkinen.

Thanks to the cleaning ladies, my day could only start well when they greeted me with a warm "Hyvää huomenta" and a grin.

SYMBOLS AND ABBREVIATIONS USED

USP Ultrashort pulse

ASTM American Society for Testing and Materials

Creq Chromium equivalent

Nieq Nickel equivalent

TABLE OF CONTENTS

1 INTRODUCTION

The constant development of new cleaning methods of the oxidation layer of the metals enables the use of new methods such as the laser, which can create the best possible readjustment of the stainless-steel layer with different settings. At the same time, a very good insight into the subject of laser technology can be realised. Most importantly, through this project one can pursue one's passion for metallurgy.

This work deals with the integration of laser cleaning, especially for weld seams, which is to be implemented in an automated process in the production flow.

For this purpose, theoretical basics on this topic will be dealt with in order to create a basis for the practical process, which includes the correct setting of the system.

1.1 Objectives

The objective of this thesis is divided into three main research questions. The main objective is to investigate the corrosion resistance of laser post-cleaned welds. For this purpose, the corrosion resistance of laser post-cleaned welds shall be found out in comparison to the 2B surface. How laser post-cleaning affects the surface topography of the welds? How this can be achieved with the correct laser machine parameters?

The analysis of laser cleaning of other materials is not taken up in this thesis. Only austenitic stainless steel EN 1.4307 is used as a material. Specifically, the weld cleaning is tested and analysed.

2 THEORETICAL BACKGROUND

2.1 Welding processes for stainless steels

Depending on the requirements, application and stainless-steel grade, the different welding processes have their advantages. The austenitic stainless steels of the 300 series, alloyed with 18-30% chromium and 6-30% nickel, are often used in manufacturing and are easier to weld, whereas super austenite, super duplex or duplex require much more attention. GTAW, gas tungsten arc welding, commonly referred as TIG (tungsten inert gas) welding is characterized by its versatility and the aesthetic appearance of the finished weld. By adjusting the current, a high-quality joint can be welded with low heat input. The process can be mechanized and used with or without filler wire (i.e. autogenous welding). For stainless steel welds, a pure argon is normally used to maintain corrosion resistance. (Trydell K., Holgersson J. 2019, 3)

PAW, Plasma Arc Welding, due to the concentrated transferred arc, narrow joints with deep bonding can be created. This usually uses argon as the shielding gas and an autogenous mechanized system. As the process is limited to a layer thickness of 8 mm, it can be used with a hybrid PAW/TIG system for a thicker filler wire. (Trydell K., Holgersson J. 2019, 3)

GMAW, gas metal arc welding, commonly referred to as MIG/MAG, is used manually or mechanized. Due to the continuous wire feed, these processes have a relatively high productivity. Depending on the material and application, different gas mixtures can be used. (Trydell K., Holgersson J. 2019, 3)

SAW, submerged arc welding, is mainly used for thicker materials since it is fully mechanized and is often used for highly productive welding of stainless steel because of the oxidation protection provided by the flux powder. (Trydell K., Holgersson J. 2019, 3)

LBW, laser beam welding, can be advantageous due to the high intensity of the laser beam with the ability to penetrate deep into semi-thick areas with little material distortion. (Trydell K., Holgersson J. 2019, 3)

2.2 Laser cleaning

Light amplification by stimulated emission of radiation (laser) is light amplification by stimulated emission of radiation. In order to use the laser for manufacturing purposes, electromagnetic radiation must be generated, and optical, mechanical and scattering components must be used for industrial applications. The laser beam serves as an energy carrier, which is guided from its point of origin to the effective zone on the workpiece with the aid of mirrors or flexible glass fibres. Depending on the requirements of the manufacturing process to be performed, the beam is shaped and focused. (Hügel H. 2009, 13-14)

In this work, PLA technology in particular was used for laser cleaning. This is a process in which material is removed from a target material by irradiation with an intense, ultra-pulsed laser beam, which is called pulsed laser ablation. The energy of the laser beam is higher than the binding energy between the atoms of the target material, so that ablation can take place. When the electrons in the target material absorb the energy of the incident photons, they transfer the energy to the phonons, i.e. the lattice vibrations, and cause the material to heat up. This sudden strong heating of the material leads to an erosion of the surface oxidation layer and thus to a vaporization of the material. (Singh A. 2020, 27-28)

Laser ablation involves removing a layer of material with the laser beam, as shown in the illustration below (Fig. 1). The beam hits the oxidation layer, breaks up the dust or rust layer and flings it away. Each material has a different ablation threshold, but the energy transmitted by the laser beam must be above this threshold. (Laserax 2020)

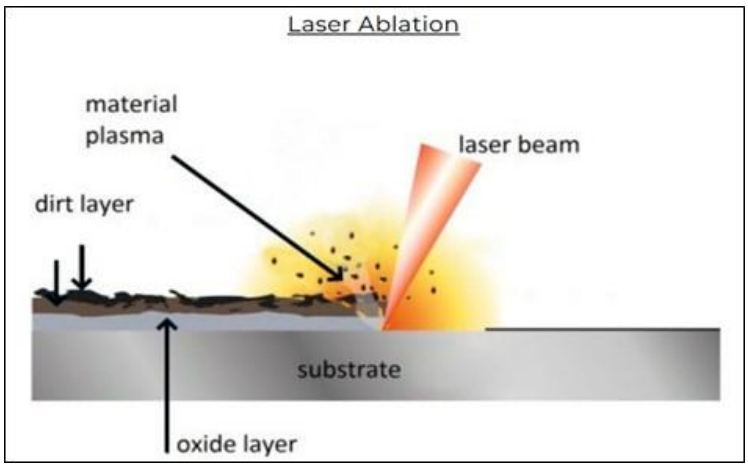

Figure 1 Principle of laser ablation (Laserax 2020)

2.3 PLA- parameters

Suitable laser parameters are important in laser cleaning processes. Therefore, several parameters need to be considered during the coating removal process: Wavelength (λ), laser fluence (F), pulse width (PW) and repetition rate. (Lee D., Cheng M. 2006, 1591–1596; Qiumei B.,Yu X., Baozhen Z., Zenghu C., Shuting L. 2013, 395–398)

An inappropriate choice of laser parameters can lead to overexposure due to the high energy density of the laser beam. Under-exposure will result in residual contamination on the surface of the substrate. Table 1 below lists the parameters and their derivation formulae for characterizing pulsed and CW laser radiation.(Heidelman G. 2009, 38–41; Jinghua H.,Xudong C.,Sha W.,Guoying F, Guoliang D., Ruifeng H. 2017, 1947–1955)

Table 1 Laser-Parameter (Georg Heidelman 2009; Han et al. 2017)

Symbol	**Definition**	**Unit**	**Formula**
τ_p	Pulse duration	s	$\tau_p = Dc/RR$
RR	Repetition rate	Hz	$RR = D_C/\tau_p$
D_C	Duty cycle	-	$D_C = RR * \tau_p$
P	Power	W	$P_{peak} = E/\tau_p$
E	Energy	J	$E = P_{peak} \times \tau_p$
A	Area of laser beam	cm^2	$A = (\pi/4) \times (diameter)^2$
I	Intensity	W/cm^2	I=P/A
F	Fluence	J/cm^2	F=E/A

2.3.1 Energy of the laser

The optical energy of the laser beam is converted into thermal energy. As a result, the laser beam interacts with the workpiece surface itself. A prerequisite for material processing is the input of laser energy because the amount and density of the energy determines the type of effect on the material. Of the coupled energy, a part is used for heating and melting the material. If the amounts of energy are dissipated by heat conduction into the interior of the component or emitted in the form of radiation to the surface of the workpiece, losses occur in the process.(Brenner A. 2021; Razab et al. 2018, 393-402)

2.3.2 Productivity increase and limitation in ultrashort pulse ablation

Thanks to the continuous development of modern laser beam sources, extremely high average laser powers of up to P_m = 8.9 kW in the ultrashort pulse range can be successfully tested in the laboratory. Commercial high-power ultrashort pulse laser beam sources have a maximum average power of 300-600W. The laser power is therefore not an obstacle to increasing the ablation rate/productivity in the USP (Ultrashort pulse) range but is limited by the high requirements for ablation precision and surface quality. In the following illustration (Fig.2), the three most important parameters are shown graphically.

Laser power can be calculated using equation (ref):

$$P_m = E_p \cdot f_{rep}$$

P_m is average laser power

E_p is pulse energy

F_{rep} is repetition rate

This results in the increase of productivity by scaling the power:

- Increase in pulse energy
- Distribution of the pulse energy over the pulse width
- Increase of the repetition rate

(Brenner A. 2021; Razab et al. 2018, 393-402)

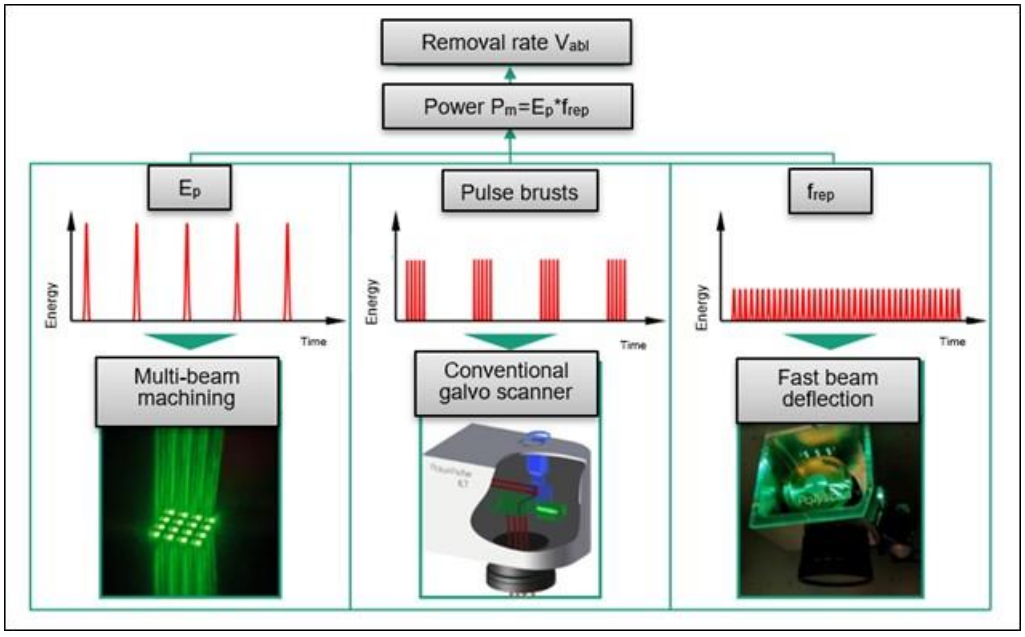

Figure 2 Ablation rate (Brenner A. 2021; Razab et al. 2018, 393-402)

2.3.3 Influence of the pulse energy

With increasing pulse energy, the achievable structural resolution decreases and at the same time the fluctuation F_o linear increases. This leads to a loss of ablation efficiency ϵA.

However, an increase in productivity can occur if the laser beam and thus also the pulse energy is divided into several to hundreds of partial beams, since the material removal can take place in parallel.(Brenner A. 2021; Razab et al. 2018, 393-402)

2.3.4 Influence of the repetition rate

An increase in the repetition rate is limited by the scanning speed v_{SCAN} of the beam deflection unit. For laser material ablation, a pulse overlap of 50-80% should be selected. A larger pulse overlap can lead to the formation of very rough microstructures on the material surface. To achieve sufficient local separation of the laser pulses, very high scanning speeds are required for power scaling with high repetition rates in the MHz range.(Brenner A. 2021; Razab et al. 2018, 393-402)

2.4 Oxidation

High-temperature corrosion, like oxidation, is any reaction of a metallic material with oxygen in which oxides are formed. The solid (metal) and a gas (oxygen) react with each other, and a solid reaction product (metal oxide) is formed. As a result, the thermodynamic stability decreases with increasing temperature.(Teneva-Kosseva G. 2005, 3-9)

Thermodynamics of metal oxidation

During the dry oxidation of a metal M, pure oxygen O_2 can be formed with the formation of the reaction product:

$$xM + \frac{y}{2} O_2 \leftrightarrow M_x O_y$$

the Gibbs free energy is given by G:

$$G = -RTln(\frac{a_{MO_2}}{a_M * P_{O_2}})$$

The activity of the metal a_M and the oxide $a_{MO_2}$is equal in the equilibrium state results:

$$G=RT*ln\ *P_{O_2}$$

In the state of equilibrium, the standard free energy depends only on the temperature and the partial pressure of oxygen P_{O_2}. If the oxygen partial pressure of the surrounding atmosphere is higher than the decomposition pressure, metal can be converted into metal oxide. (Zimmermann D. 2001, 16-20)

2.4.1 Oxidation mechanisms

For the formation of the metal oxide layers, a distinction is made between a start-up period and a phase of diffusion-controlled scale growth. During the start-up period, various processes occur at the phase interfaces. First, a non-epitaxial, polycrystalline oxide primary film is formed, and monocrystalline, epitaxial oxide nuclei are formed. A compact oxide layer is formed due to the growth of oxide nuclei; this oxide layer is a few hundred nm thick.

During mass transport through the oxide layer and due to the oxide formation reaction taking place at the phase boundary, scaling of the metal occurs.

The following mechanisms are possible for ion exchange, as shown in figure 3:

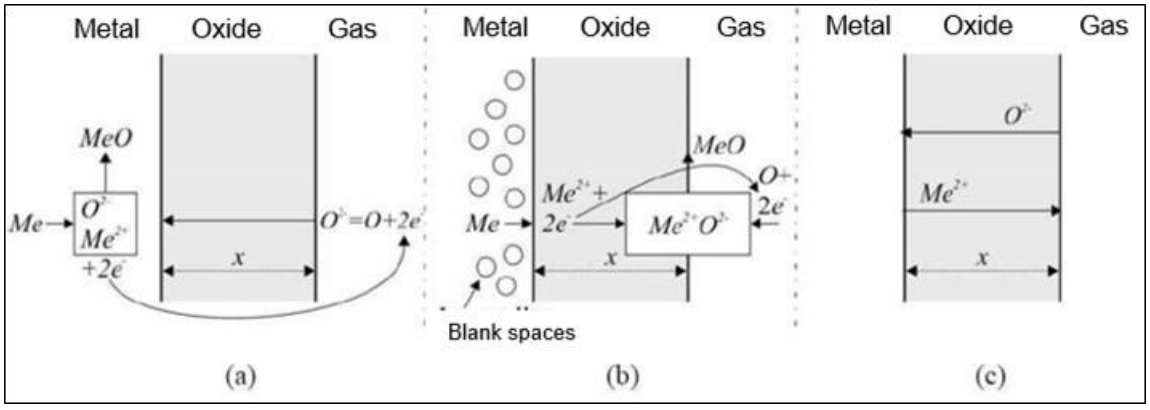

Figure 3 Oxidation mechanisms (Katsich C. 2010, 20-21)

Metal/oxide, layer growth takes place at the interface, mass transfer takes place through diffusion of the oxygen ions. Since the reaction front is sharply defined, this penetrates the material and is therefore referred to as "internal oxidation". Oxide/gas, the layer growth at the interface, where the diffusion of the metal cations from the material through the oxide layer to the phase boundary takes place, is called "external oxidation". (Katsich C. 2010, 20-21; Simon D. 2019)

With simultaneous layer formation and combination of diffusion processes at the phase boundaries, the layer growth takes place at the metal/oxide and oxide/gas interface.

The transport of the reaction partners through the scale layer can take place via cation diffusion or anion diffusion via defects in the ion lattice of the scale. Possible lattice defects can be cation vacancies, cations on interstitial sites, anion vacancies and anions on interstitial sites. The charge is balanced by more highly charged cations or free electrons. (Katsich C. 2010, 20-21; Simon D. 2019)

2.4.2 Oxidation in welding of austenitic stainless steel

When a hot metal surface is exposed to oxygen in the atmosphere, a surface oxide is formed. This results in a visible discoloration of the metal surface due to the oxides, known as "heat discoloration" or “heat tint”. The surface oxides formed during welding reduce corrosion resistance, especially in chloride-containing environments.

The reduced corrosion resistance depends on the properties of the oxides:

- Chemical composition
- Inhomogeneous microstructure
- Composition of the alloying elements of the base metal

For austenitic stainless steels a temperature of approx. 450°C is required for the formation of oxides, which can have a negative effect on corrosion resistance. To avoid a reduction in corrosion resistance, the oxide content of the environment should be controlled to reduce oxidation during welding. The root side should be shielded as much as possible during welding to prevent the formation of surface oxides. (Turan J. 2018)

2.4.3 Behaviour Influence of alloying elements on oxidation behaviour

Chromium (Cr)

The chromium (Cr) content in the alloy helps to improve oxidation/corrosion resistance by forming a protective, adherent, slow-growing Cr_2O_3 oxide layer (chromium oxide). The function of the oxide is that it grows slowly and blocks the diffusion of chromium (Cr^{3+}) outwards along the grain boundary. This happens faster than the diffusion of oxygen. At lower chromium contents, the spinel oxide $FeCr_2O_4$ forms, which is less protective. The higher the chromium content in the alloy, the greater the resistance to oxidation.(Simms H. 2011, 6-7)

Silicon (Si)

The addition of silicon (Si) is an important factor in the oxidation resistance of stainless steels. Silicon facilitates the initial formation of the chromium oxide layer and the silica particles prevent the diffusion of chromium ions to the outside under the chromium oxide layer. In optimum amounts, silicon and chromium can improve oxidation resistance without affecting creep resistance.(Simms H. 2011, 6-7)

Manganese (Mn)

Manganese (Mn) can have a positive or negative effect on oxidation resistance. It can form spinel, which is detrimental to oxidation resistance.(Simms H. 2011, 6-7)

Nickel (Ni)

Nickel (Ni) can reduce cation diffusion in the Cr_2O_3 layer, preventing the formation of Cr_2O_4+Fe_2O_3, which in turn affects the mechanical adhesion properties. Nickel has a positive influence on repassivation and reduces the rate of pitting corrosion.(Simms H. 2011, 6-7)

Molybdenum (Mo)

Molybdenum (Mo) is the most important alloying element for stainless steels after chromium. The resistance to pitting and crevice corrosion can be increased in media containing chloride. Especially for pitting corrosion resistance, molybdenum has a higher effect than chromium by a factor of 3.3. With molybdenum, the resistance to stress corrosion and the heat resistance can be increased. (Simms H. 2011, 6-7)

Copper (Cu)

Copper (Cu) can increase corrosion resistance in certain acids and promote austenitic microstructures. Strength can be increased by copper forming intermetallic compounds. (Simms H. 2011, 6-7)

Carbon (C)

An austenitic structure can be promoted by carbon (C), which also increases mechanical strength. Resistance to intergranular corrosion can be reduced by carbon. This is because at elevated temperatures, chromium carbides are formed, which are preferentially deposited at the grain boundaries. This leads to embrittlement of the material and sensitisation to intergranular corrosion. In martensitic stainless steels, however, carbon with a content of 0.7 % is a useful alloying element that contributes to the hardenability of the material.(Informationsstelle Edelstahl Rostfrei 2023)

Aluminium (Al)

In stainless steels, aluminium (Al), like silicon, is added to represent the oxygen dissolved in the steel in the form of aluminium oxide. The formation of firmly adhering aluminium oxide layers can improve the scaling resistance of heat-resistant ferritic steels. In this process, the scaling process is delayed under the influence of an oxidising gas atmosphere.(Informationsstelle Edelstahl Rostfrei 2023)

2.4.4 The influence of alloying elements on the microstructure

The alloying elements can be divided into ferrite (α) stabilisers and austenite (γ) stabilisers. This means that the formation of ferrite or austenite is favoured in the microstructure. If the ability of the austenite stabilisers to promote austenite formation is related to nickel and the ferrite stabilisers are also related to chromium, the total ferrite and austenite stabilising effect of the alloying elements in the steel can be calculated. These results in chromium (Creq) and nickel (Nieq) equivalents are often summarized in the "Schaeffler diagram" (Fig.4). Cr- and Ni-equivalents are calculated with the following equations:

- Creq = %Cr+1,5*Si%+%Mo
- Nieq = %Ni + 30 x (%C+%N) + 0,5 x (%Mn+%Cu+%Co)

Thus, the combined effect of the alloying elements can be considered.(Leffler B. 2013, 4-9)

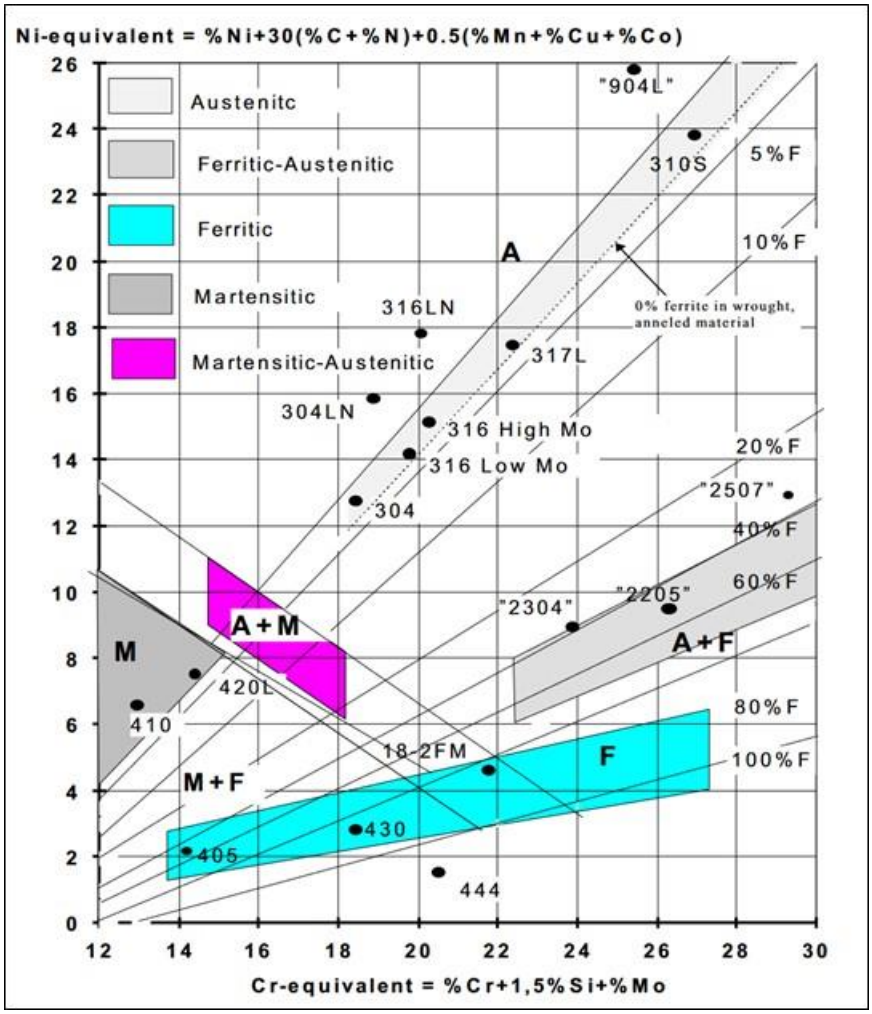

Figure 4 Schaeffler Delong diagram (Leffler B. 2013, 4-9)

2.5 Different ways corrosion can occur

Corrosion can occur in three different ways: uniform attack, localized attack, and localized attack associated with mechanical stress. The following figure 5 briefly explains the different types of corrosion. (Kämmerer B. 2012, 17–26)

Point of attack	**Corrosion phenomenon**	**Schematic**
Uniform	Surface corrosion under: Hydrogen evolution Oxygen consumption	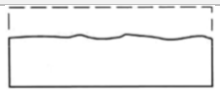
Local attack	Crevice corrosion	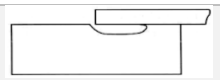
	Pitting corrosion	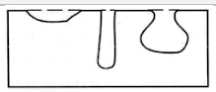
	contact corrosion: Component of different materials Heterogeneous microstructure	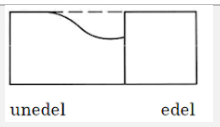
	Intergranular corrosion	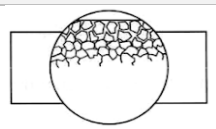
Local attack in combination with mechanical stress	Stress corrosion cracking (Static load) Fatigue corrosion cracking (Dynamic loading)	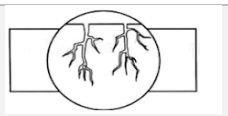
	Erosion Corrosion	
	Cavitation corrosion	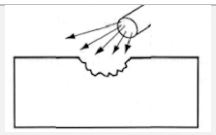
	friction corrosion	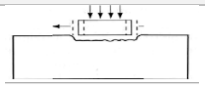

Figure 5 Different types of corrosion (Kämmerer B. 2012, 17–26)

2.5.1 Mechanisms of pitting corrosion

The passive surface, which serves as a passive layer, is more noble than the underlying material. If the passive layer is locally breached without being immediately passivated again, a small active area (anode) prevails next to a large cathodic area (passive layer). Due to the large area difference, large anodic current densities can occur, causing holes to form quickly and deeply. Pitting corrosion can only occur due to the presence of specific ions, such as halide, perchlorate, or sulphate ions.

Pitting corrosion can occur in three different forms, which are listed in the figure 6 below. (Kämmerer B. 2012, 17–26)

Extent of pitting corrosion	Cross section of pitting corrosion
Maximum extension visible from above	
Maximum extension not visible from above	
Direction of maximum extension	

Figure 6 Three different forms of pitting corrosion (Kämmerer B. 2012, 17–26)

Pitting corrosion in passive metals can be divided into two phases:

1. pitting initiation (local failure of the passive layer).

2. pitting growth (formation of stable holes).

Pitting nuclei can be minute structural perturbations of the surface layer, on the order of impurity inclusions, breakouts, or dislocations.(Kämmerer B. 2012, 17–26)

There are three different attack mechanisms for the destruction of the passive layer. These are divided into penetration mechanism, island adsorption mechanism and layer cracking mechanism. (Suter T. A. 1997, 123-132)

Penetration mechanism

The migration of chlorides through the passive film to the metal/film phase boundary is the key step. The penetrated chlorides compete with hydroxide ions. The salt compounds create localized pathways with high conductivity, as shown in the figure below. During this process, the passive layer loses its protective effect. However, in an EU research program (COST 502), it was found that no chlorides migrated through the passive film. Hole formation after the penetration mechanism was thus ruled out, as in the figure 7. (Suter T. A. 1997, 123-132)

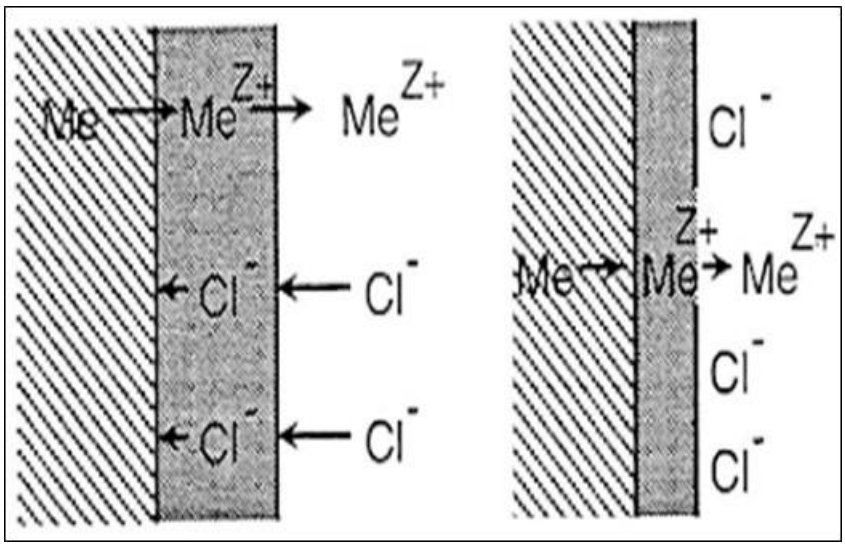

Figure 7 Penetration mechanism (Suter T. A. 1997, 123-132)

Island adsorption mechanism

Chlorides are adsorbed at energetically preferred sites, and potential-controlled accumulation occurs. The adsorbed chlorides cause a dilution of the passive film and thus an increase of the metal ion transfer into the corrosive medium. The chemisorbed O^{2+} ions are displaced, and Cl^- ions take their place. The increased electric field strength within the passive film causes an increased migration of the metal ions, seen in the following figure 8. (Suter T. A. 1997, 123-132)

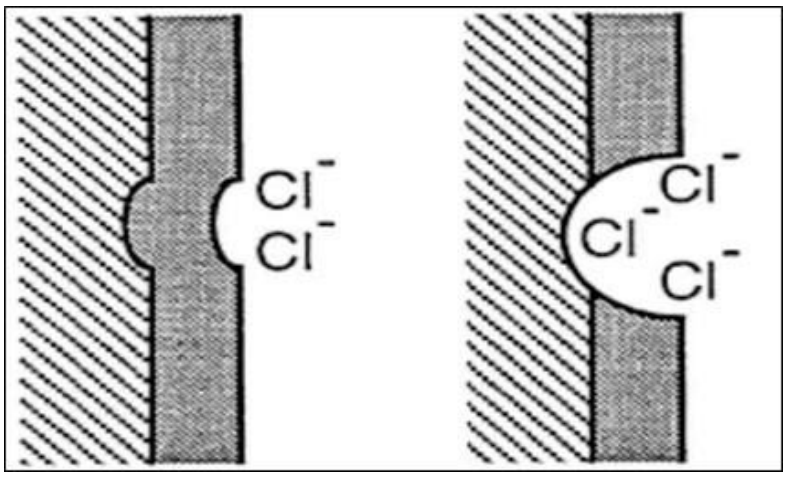

Figure 8 Island adsorption (Suter 1997, 123-132)

Mechanism of film cracking

Here, compressive and tensile stresses are assumed to cause local deformations in the passive film. The film cracks when the strength of the film is no longer sufficient at one point. Stress sources are: Interfacial stresses, electrostriction pressures due to the high electric field in the film, internal stresses, and local stresses, as seen in figure 9. This mechanism requires the presence of an aggressive electrolyte, since passivation is a very fast process, and the film would otherwise heal more easily. (Suter T. A. 1997, 123-132)

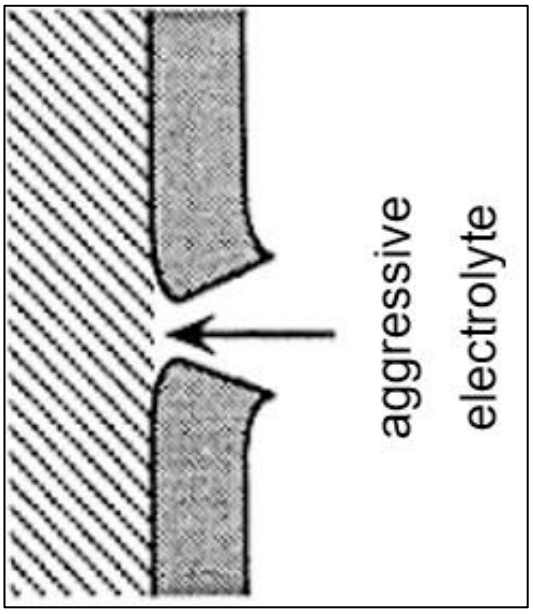

Figure 9 Film cracking (Suter T. A. 1997, 123-132)

2.5.2 Hole growth

Stable hole growth i.e. progression of pitting corrosion can start by local destruction of the passive layer. A large cathodic passive region faces the active anodic hole core. Immediate repassivation can be prevented by two fundamentally different variants. (Suter T. A. 1997, 123-132)

Salt film formed at the bottom of the hole causes an ohmic voltage drop. Since the potential of the hole core is in the active region and the rest of the surface is passive, the potential difference between the active and passive regions can be several hundred mV.

The most important factor however, is the pH decrease in the hole core caused by the hydrolysis of the dissolved metal cations.

The anodic metal dissolution:

$$Me \rightarrow Me^{2+} + 2e^{-}$$

The hydrolysis:

$$Me^{2+} + nH_2O \rightarrow Me(OH)_n^{(2-n)+} + nH^{+}$$

The higher H+ concentration allows accelerated migration of chlorides into the hole cores and hydrochloric acid is formed:

$$Me^{2+} + nH_2O + nCl^{-} \rightarrow Me(OH)_n^{(2-n)+} + nHCl$$

The hole growth progresses more and more as the electrolyte becomes more aggressive, so that the hole corrodes autocatalytically. The maximum corrosion rate depends on the diffusion rate and the migration rate of the ions involved. (Suter T. A. 1997, 123-132)

The following gives an example of the formation of a metastable hole.

It was assumed that the formation of hole nuclei occurs at imperfections, such as non-metallic inclusions in the surface, see all steps in the figure 10 below.

1. Repassivation:

Active metal dissolution can occur due to charge balance in the passive layer. Repassivation occurs when this charge balance cannot be maintained.

2. Stable pitting (salt film):

Active metal dissolution can occur when chloride ions are deposited on the metal surface during passive layer injury and form a salt film, allowing charge balance to be maintained.

3. Stable pitting (crevice type):

When the metal dissolves near soluble non-metallic inclusions, active dissolution occurs due to the crevice effect of the void formed, even with a lower charge balance.

4. Crevice Corrosion:

Low charge balance can lead to localized metal dissolution because there is little exchange of electrolytes in the gap. (Kämmerer B. 2012, 17–26)

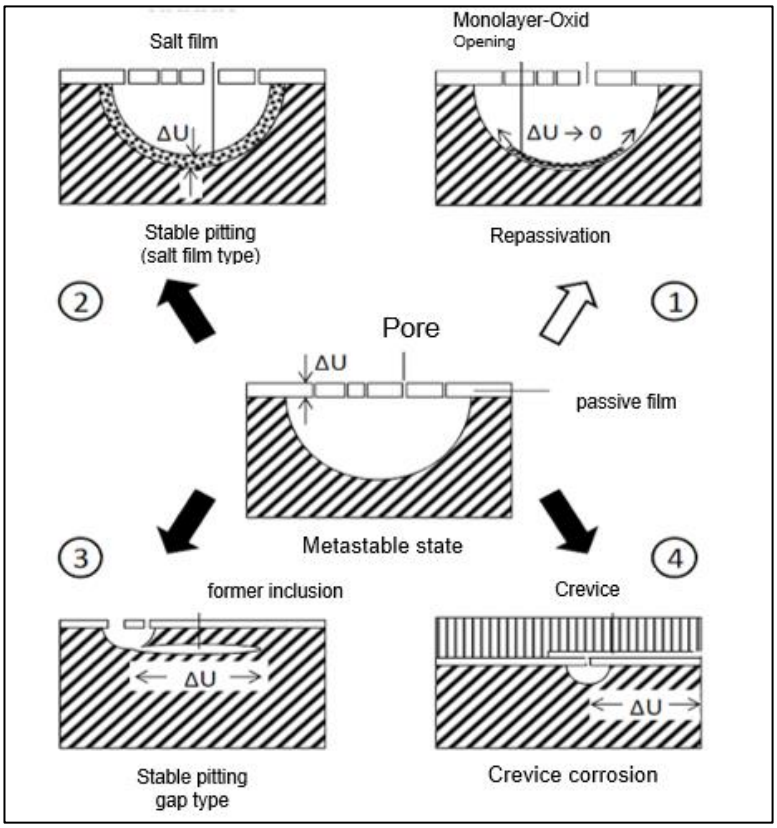

Figure 10 Formation of a metastable hole (Suter 1997, 123-132)

2.6 Temperature effect on the passive layers

Increasing temperature causes oxide layers to form on the stainless steel surfaces. This disadvantageous oxide layer must be removed by cleaning processes such as pickling, sandblasting, grinding, etc. Oxidation is kinetically controlled by diffusion processes. For this purpose, oxygen must be adsorbed and dissociated at the interface between the environment and the oxide layer. Metal ions can diffuse interstitially into the oxide or along the grain boundaries into the oxide layer and onto the surface. Growth of the oxide layer is possible both inward and outward.

As the temperature increases, the kinetic and thermodynamic processes are affected, resulting in a change in the oxide layer system. Other factors are chromium content, oxygen partial pressure, humidity, and passivation.

Visually, the influence of temperature can be seen in so-called tarnish colours (Fig. 11); the coloration of the surface can be explained by the extinction of individual wavelengths due to destructive interference of the incident light. The colour provides information about the chemical compositions and associated calculation indices of the oxide layer on the layer thickness. The following figure 11 shows the tarnish colours of various tools as a function of chromium content, aging temperature, and time. (Kämmerer B. 2012, 17–26)

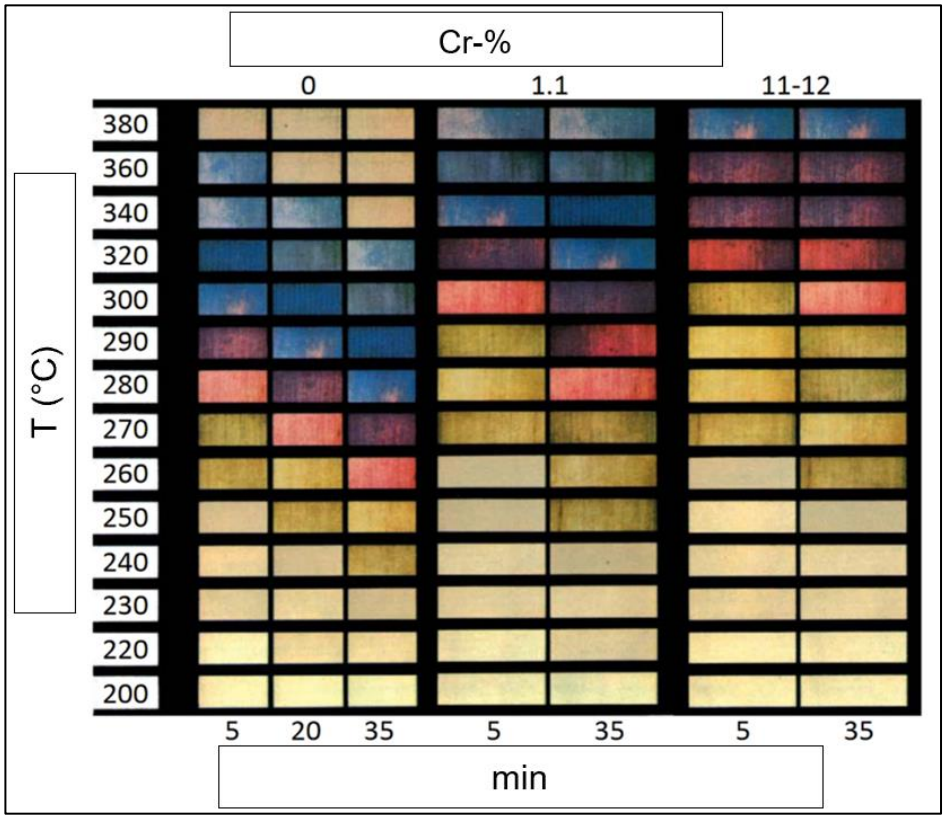

Figure 11 Effect of Temperature (Kämmerer B. 2012, 17–26)

Welding oxidation is caused by a thickening of the originally thin chromium-rich oxide passive layer on the surface. Compared to the original state, the thicker layer has a scale-like film, which can lead to chromium depletion in the underlying material during formation. (Trydell K., Holgersson J. 2019, 23-24)

Different types of cleaning processes and surface treatment after welding

In mechanical treatment of stainless steel weld, the cleaning methods are divided into shot blasting, polishing, sandblasting and brushing. Mechanical treatment is much more environmentally friendly and not as harmful to health as chemical treatment. However, it leads to rougher and uneven surfaces, which in turn is less efficient.(Laren M. 2004, 95-100; Westin E. M. ,Olsson C.-O.A, Hertzman, S. 2008, 2620-2634)

Passivation, electropolishing and pickling are used for chemical post-treatment. This process is much more efficient, especially when it comes to removing the effects of heat and restoring the corrosion resistance of steels. The pickling bath requires a mixed acid mixture of nitric acid (HNO_3) and hydrofluoric acid (HF). (Laren M. 2004, 95-100; Westin E. M. ,Olsson C.-O.A, Hertzman, S. 2008, 2620-26340)

Laser ablation is an exclusively dry procedure; the ablation mechanism does not require any additional solutions. Simple and precise local treatment of surfaces can be performed. (Trydell K., Holgersson J. 2019, 23-24)

3 MATERIALS AND METHODS

3.1 Test material

Used test material was EN 1.4307/AISI 304L which is an austenitic stainless steel. It is widely used in applications requiring moderate corrosion environments.

Low carbon content minimizes carbide precipitation as a result of heat input, for example during welding, giving improved resistance against intergranular corrosion. Pitting and crevice corrosion may occur in chloride environments. Stress corrosion cracking can occur above 60°C. (Outokumpu 2023)

In Table 2 a typical chemical composition for the test material is given. Chemical composition is taken from steel manufacturer's data sheet.

Table 2 Chemical composition of the test material. (Outokumpu 2023)

C [%]	Mn [%]	Si [%]	P [%]	S [%]	Cr [%]	Ni [%]	N [%]
0,03	2,0	1,0	0,045	0,03	17,5-19,5	8-10,5	0,1

Figure 4 shows the chromium equivalent and nickel equivalent properties of material 304, where the material is in the ferritic-austenitic range.

3.2 Overview of used test methods

For the analysis of the metal samples, which had previously been cleaned with different laser parameters, they were subjected to six different types of experiments shown in Fig. 12. All experimental methods are described more detailed in later chapters.

For this purpose, a duplicate of each sample was made in advance so that the initial product could always be analysed.

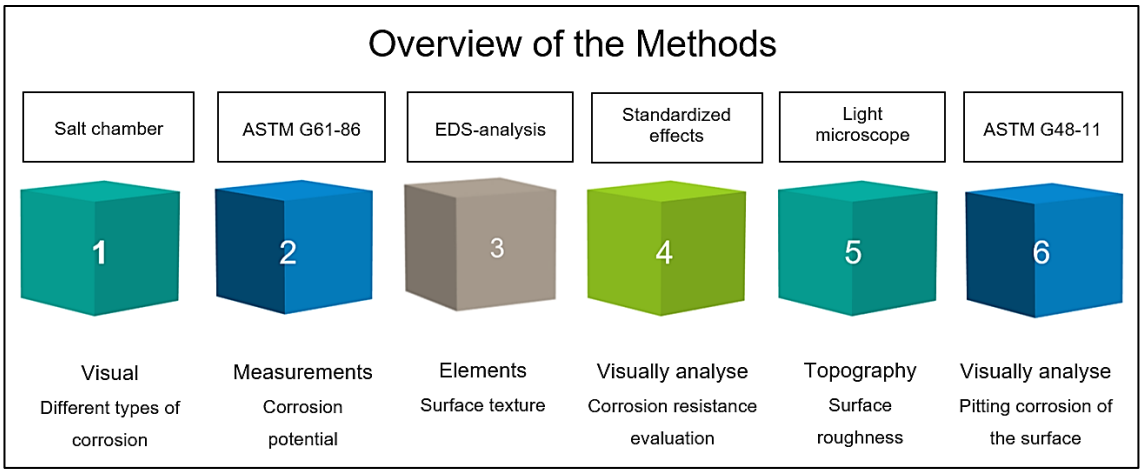

Figure 12 Overview of the different experiments

3.3 Studied laser parameters

The goal was to determine which settings of the laser had the greatest influence on the removal of the oxidation layer, which could be analysed from the results. In the first run which was designed for screening, seven different variables were studied. After that, four most significant variables were selected by the Pareto principle, which is described in chapter 4.6. Plackett-Burman design was used in determining the 2nd experimental matrix. Based on the statistical model determined from the 2nd run the 3rd round experiment was designed to validate the results.

The importance of the laser variables could also be seen from the figure 13.

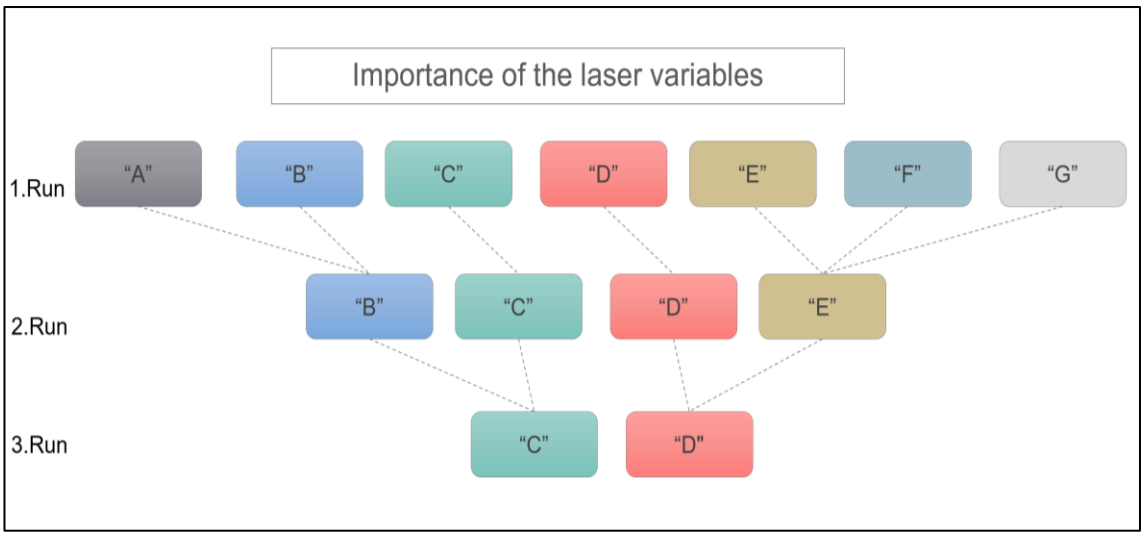

Figure 13 Laser variables used in laser cleaning experiments.

3.4 Statistical software Minitab® 20.3

Test matrices were designed with the statistical software "Minitab® 20.3". The ready-made parameter settings were predefined by the partner company "Cajo Technologies". In total, there were seven variables to set at the beginning of the laser cleaning experiments. After each test run, the overall results were entered into the matrix based on the analyses of how well these settings of the laser performed. This helped determine which parameters had the most positive impact on the corrosion resistance of the samples. For the next test run, the parameter settings with the most influence were analysed with two to four different values. Finally, the "Minitab® 20.3" software made it possible to determine the correct values for the respective laser cleaning settings in a simple and straightforward way.

3.5 The 1st Screening Matrix

During the first test run, a total of seven variables were specified by the company, which served as the basis for all further test runs. Screening matrix is given in the table 3. With the help of the screening matrix, it was possible to quickly find out which settings were relevant. For the screening matrix, three different value ranges were applied: "Low (-1)", "Medium (0)" and "High (1)".

Table 3 Screening Matrix for the first run

RunOrder	A	B	C	D	E	F	G
1	1	-1	0	-1	1	1	1
2	1	-1	1	1	-1	-1	1
3	1	1	1	0	-1	1	-1
4	0	-1	-1	-1	-1	-1	-1
5	-1	1	0	1	-1	-1	-1
6	-1	-1	-1	0	1	-1	1
7	-1	-1	1	1	1	0	-1
8	1	1	-1	-1	-1	0	1
9	0	1	1	1	1	1	1
10	1	1	-1	1	1	-1	0
11	-1	-1	1	-1	-1	1	0
12	-1	0	-1	1	-1	1	1
13	-1	1	-1	-1	1	1	-1
14	-1	1	1	-1	0	-1	1
15	0	0	0	0	0	0	0
16	1	0	1	-1	1	-1	-1
17	1	-1	-1	1	0	1	-1

3.6 The 2nd Optimization Matrix

The setting parameters that had the most positive influence on corrosion resistance in the first "screening run" were analysed further in the second "Optimization matrix" which is given in table 4. Therefore, four variables were tested with two levels. A total of four different variable settings were used with two levels "Low" and "High". Due to the previous screening matrix, fixed values could be used for three parameter settings: high “A”, low “F” and low “G”.

Table 4 Optimization Matrix of the second run

RunOrder	C	B	D	E
1	1	-1	1	1
2	-1	-1	-1	-1
3	-1	-1	-1	1
4	-1	1	-1	-1
5	-1	1	-1	-1
6	1	1	-1	1
7	1	-1	1	1
8	-1	1	1	1
9	-1	-1	-1	-1
10	1	-1	1	-1
11	1	-1	-1	-1
12	1	-1	1	-1

13	-1	1	1	-1
14	-1	1	1	1
15	1	1	-1	1
16	-1	-1	1	1
17	1	-1	-1	-1
18	-1	-1	-1	1
19	-1	1	1	-1
20	1	1	-1	1
21	-1	-1	1	1
22	1	1	1	-1
23	1	1	1	-1
24	1	1	-1	1

3.7 The 3rd Evaluation Matrix

For the final matrix, only two parameters were analysed with different values of "Low", "Medium" and "High", see in table 5. In total, the laser machine could be set with fixed values for five parameters based on the two previous test runs.

Table 5 Final Matrix of the third run

RunOrder	C	D
1	-1	1
2	1	1
3	1	0
4	-1	-1
5	-1	0
6	0	0
7	0	1
8	1	-1
9	0	-1

3.8 Welded samples

The material used for the samples was EN 1.4307 plates with a thickness of 4 mm. First, the 1250 x 600 mm^2 plate was cut into 600 mm long and 200 mm wide sheets with the plasma cutter. Then 4 pcs of 600 mm long welds were welded onto each of these sheets. A total of 13 pcs so-called narrow strips, each 600 mm long, were welded with Fronius TPS3200CrNi MAG-welding system. The following settings were used in welding: I = 100 A, U = 19 V and v = 44 cm/min. The narrow strips were cut into six specimens, each 100 mm long, as shown in the figure 14. However, as the metal pieces became thicker due to welding, 20 mm had to be cut away from each sample. Otherwise, the sample could not be placed properly in the salt chamber. Furthermore, for reasons of work safety, all edges had to be rounded and all residues from cutting the metal plates had to be removed. Finally, the surface of all samples was carefully cleaned with a dry cloth to remove any dust, see figure 15.

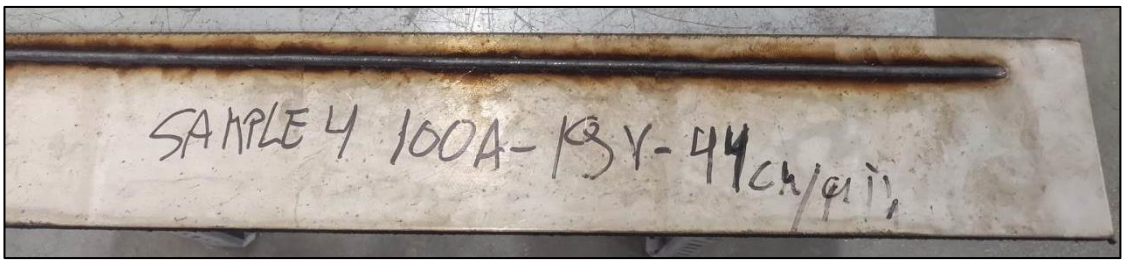

Figure 14 Metal sample after welding

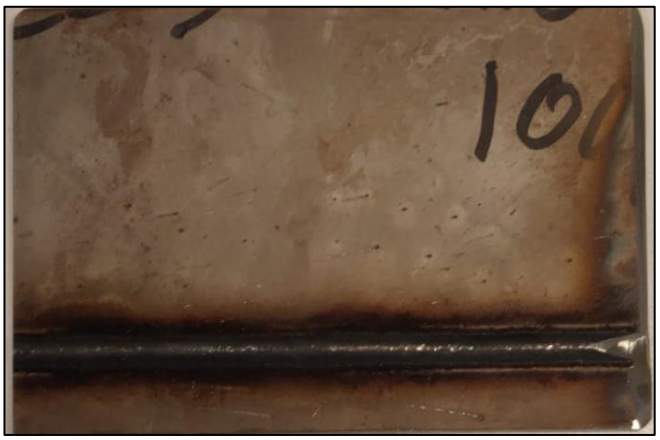

Figure 15 Finished metal sample for laser cleaning.

3.9 Laser Cleaning

For the sample production, the first tests were carried out with Cajo's 60-watt laser machine. For the further runs, however, a 20-watt laser machine was always used. For this, the minimum limit values and the maximum limit values of the settings had to be analysed in advance. This was done visually assessing whether this value could fulfil the measures.

Once all the settings were selected, a sketch of the respective trials was drawn according to the matrix.

After all the experiments had been completed, the implementation could begin, and all the experiments were carried out without any problems. A 60-watt laser machine was used for the first experiment, see figure 17 and a 20-watt laser machine for the second, third and fourth experiments, see figure 16.

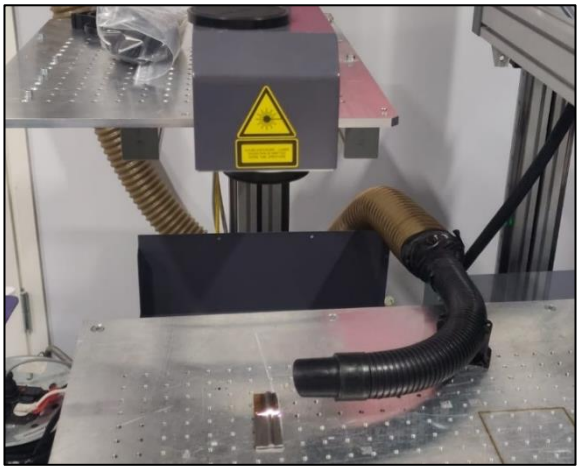

Figure 17 60-watt laser machine

Figure 16 20-watt laser machine

To check whether everything had been set correctly, all cleaning tests were lasered onto a metal piece in a small format, see figure 18.

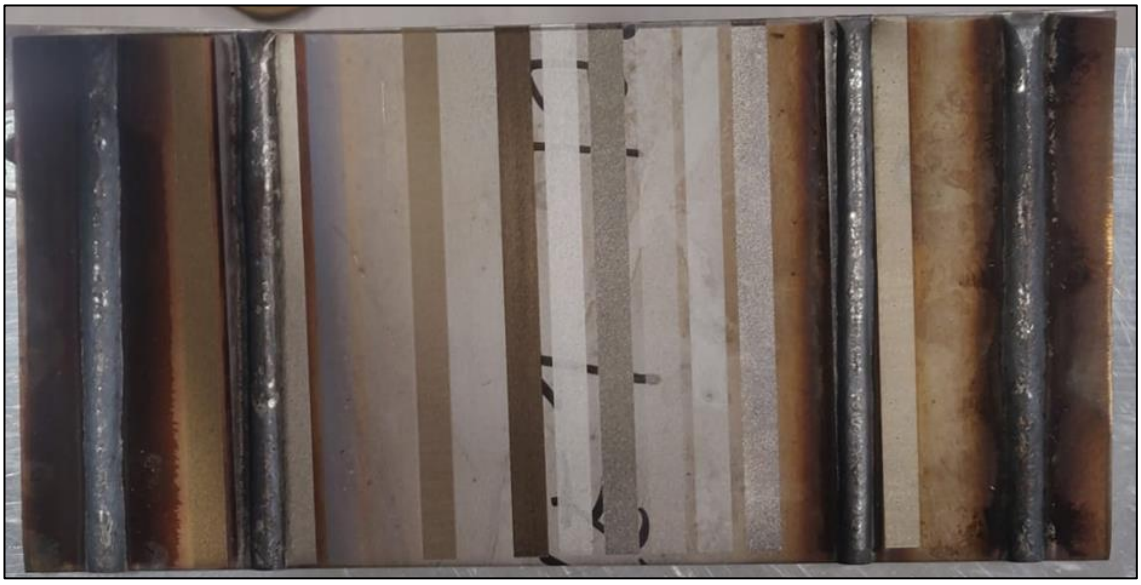

Figure 18 Check-up of the settings

As a crowning conclusion to the sample preparation, a cross-section of the samples was taken in a stab-like manner. With the metal cutter a small sample of 40 mm length was cut to have a standardised Light microscope sample later, which was then ground (grit size: #320, #600 and #1000) and polished with 3 µm and 1 µm diamond suspension. Finally, the samples were electrically etched with a 10% oxalic acid using current density of 1,5 A/cm^2. Under the light optical microscope, it became obvious that all samples revealed an identical weld microstructure with no welding imperfections. This ensured a high-quality test series.

3.10 Visual inspection

For the visual inspection (VI) of the samples, a classification of the surfaces with the scale of 1 - 10 was determined. Prior to the salt spray tests the cleanness of the laser cleaned surfaces were estimated in a way that grade 1 represented the worst cleaning and grade 10 represented the best cleaning result. Similarly, after salt spray tests if a sample received a score of 10, this meant that no corrosion was visible to the naked eye. The score 1 means that this sample had by far the most corrosion on the surface.

3.11 Criterion for the sample analysis

In total they were about 40 different combinations of values with different settings used for laser cleaning of the oxidation layer. So many samples were generated that it was not possible to analyse each sample for all tests. Therefore, only three to four samples could be analysed in each test run. The samples after the salt spray test with the best corrosion resistance, the samples with the worst corrosion resistance, and the samples with average corrosion resistance were used. These three to four samples were then used for all five tests. To be able to test the influence of the laser cleaning, a REF (reference), which was the sample, with only the weld without laser cleaning was used for. In this way, a good compact overall result could be determined.

3.12 Salt spray tests

SFS-EN ISO 9221 (Corrosion tests in artificial atmospheres. Salt spray tests) is a salt spray test used to provide information on the relative corrosion resistance of samples of metals and coated metals exposed in a standardised corrosive environment.

Prior to this, the entire salt chamber had to be cleaned so that the residue from the previous test runs would not interfere with a new test batch. All samples were placed in the cabin at even intervals as shown in the figure 13. All samples were sprayed with a 5% salt solution at a temperature of 35°C to inject pitting into the samples. After one week, the first visual inspection took place, after which the response for each run defined in test matrix was determined with visual inspection given in the previous chapter. After that "Pareto diagram of standardized effects" was determined with the Minitab®. Now it was clear which parameters had an influence on the removal of the oxidation layer and increased the pitting resistance.

As an indicator, a reference metal sample was placed untreated in the salt chamber. In addition, another metal sample was ground with the flex to later visually check whether this is a better cleaning of the oxidation layer than laser cleaning.

During the first test run, the samples were placed in the salt chamber, see figure 19, so that the front side i.e., side with the reinforcement was covered with the solution. In the subsequent test runs, the samples were placed with the back side facing the spray nozzles. This was done so that it could be determined later whether the required inert gas could be omitted during the welding process.

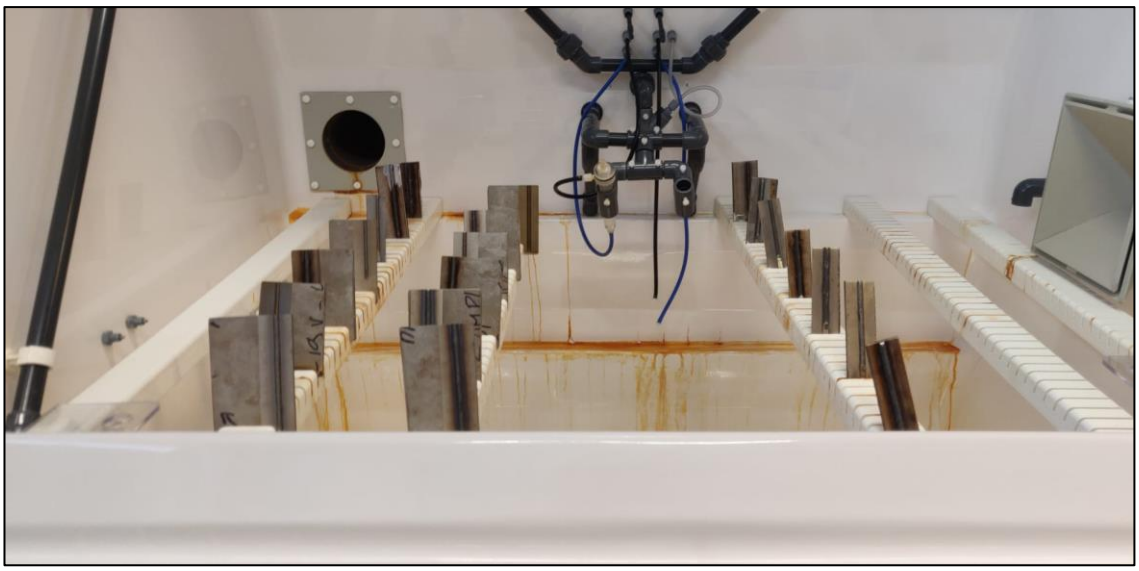

Figure 19 The metal samples of the first run

3.13 Pitting corrosion potential measurements

At the same time, the same samples were analysed in the Avesta cell according to the requirements given in standard ASTM G61-86 (Standard Test Method for Conducting Cyclic Potentiodynamic Polarization Measurements for Localized Corrosion Susceptibility of Iron-, Nickel-, or Cobalt-Based Alloys) E_{corr} and i_{corr}. The rating CR (Corrosion rate mm/year) is not included in ASTM G61-86 but can be calculated from the E_{corr} and i_{corr} values. To determine later which setting was the most corrosion resistant. For the Avesta cell shown in the figure 20, the filter paper was first placed in the grooves at the bottom of the Avesta cell. Then the sample was clamped into the opening below, with a suitable O-ring having to be selected beforehand. The sample was clamped in place using the holder and the cable connection was also clamped in place, ensuring contact with the sample. This leads to a sealing of the bottom and the Avesta cell can be filled up to approx. 70% with a 3.56% NaCl solution. However, only a little should be filled in at the beginning, as the connection with the sample may not have been tight enough.

The water pump was connected to the apparatus and had a flow rate of 3 mL/h. Distilled water was pumped into the cell. The mixer had to be inserted before the lid was mounted. Two graphic counter electrode rods as well as the reference electrode (a calomel, probe tip approx. 1 mm from the working electrode) could be inserted into the openings. Finally, the gas dispersion sensor could be positioned provisionally, whereby it is important that not too much gas flows in, otherwise the measurement can be strongly influenced. For one hour, the solution was enriched with a suitable gas to remove the oxygen. Another hour was needed because in addition to the gas, the mixer was switched on to distribute the gas evenly. Now the programme "Cycle Polarization" could be selected and started. This varied depending on the sample, because the measurement is finished when the corrosion process has been measured.

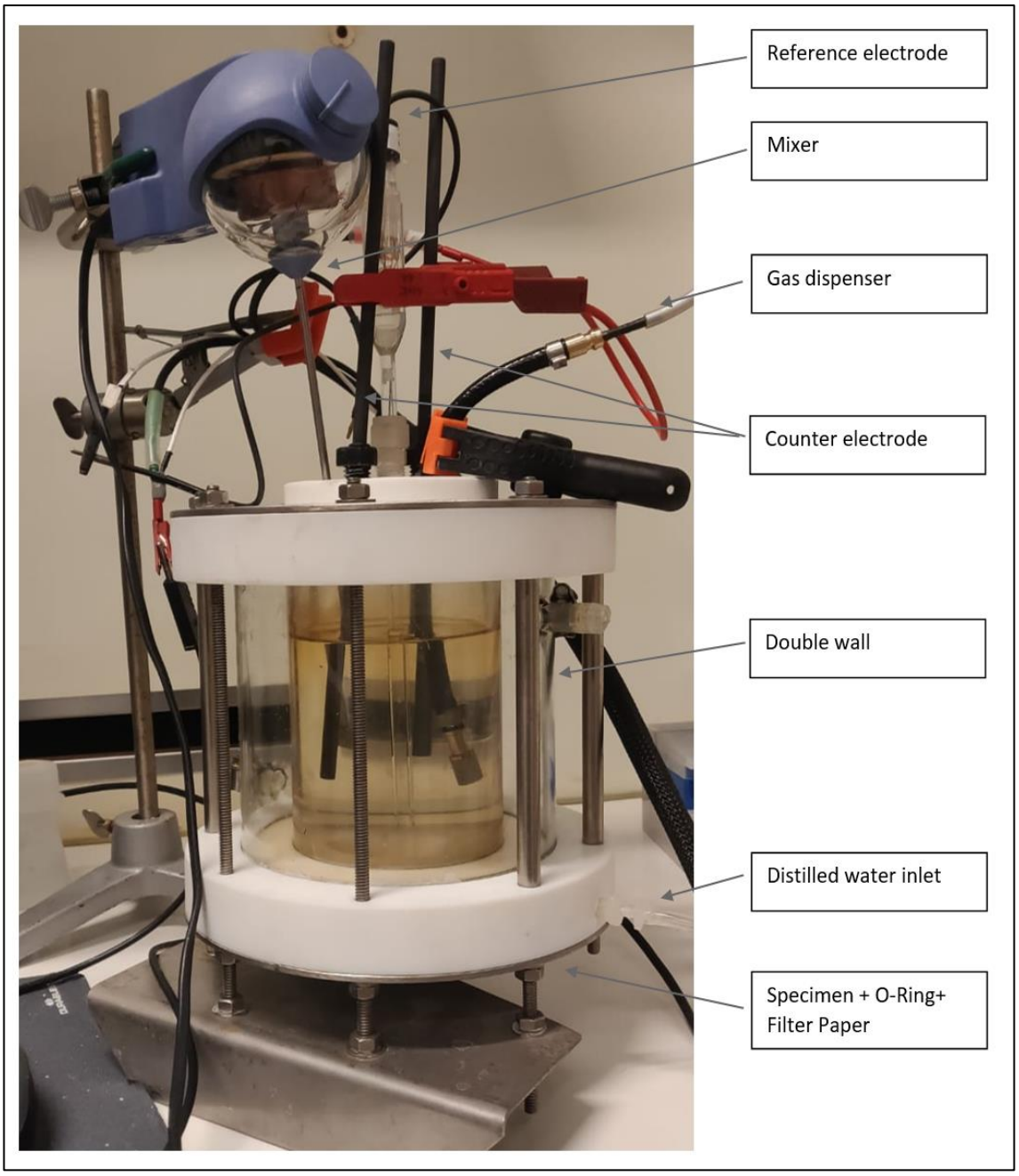

Figure 20 The equipment of the Avesta cell

3.14 EDS-analysis

Energy dispersive X-ray spectroscopy (EDS) is a measurement method in materials analysis that belongs to X-ray spectroscopy. The atoms in the sample are excited by an electron beam of a certain energy; they then emit X-ray radiation of an energy specific to the respective element, the characteristic X-ray radiation. This radiation provides information about the elemental composition of the sample.

To do this, the Quanta FEG 450 microscope must first create a vacuum in the sample chamber. Then the correct height of the stage was set for the sample. So that the reflection develops its optimum effect. To get a sufficient overview of the surface, the following settings were chosen: 6.50 kV, 100 x magnification and a spot size no 2. The magnified surface was able to accurately reproduce the angles of the laser irradiation. For the EDS-analysis, a voltage of 20 kV was used to determine the amount of elements from the material.

The Quanta FEG 450 microscope was again used for elemental analysis of the surface. Incident electron beams were excited and emitted by the atoms of the sample. The emitted characteristic X-rays have specific wavelengths.

Thermo Nora System 312E EDS integrated Quanta 450 FEG FESEM

To perform energy dispersive X-ray spectroscopy, the software "Thermo Nora System 312E" is used, which displays the composition of the elements found from the sample.

3.15 Standardized effects

Using the Pareto principle, the corrosion resistance of the metal samples could be quickly and easily analysed visually. In the visual analysis "Pareto diagram of standardised effects", all samples of the respective test were given a score from 1 to 10, with 10 representing the best possible visual result that was possible with the laser cleaning. In this way, the "Minitab" programme was able to graphically represent which properties have the greatest influence on corrosion resistance.

3.16 Light microscope

With the help of a light microscope, the topography of the samples could be analysed, and a visual simulation of the sample could be created. For this purpose, the surface was scanned in individual sections. Leica DMI 5000M reverse light microscope was used for the investigations.

The samples had to be cut to the correct sample size beforehand. Then the sample was pressed with a filling material to the required standard of the sample size. Subsequently, the samples were ground evenly with the filter paper. A 200x magnification was used under the microscope as this provided the best possible image quality for the topography. By visualising the topography, it was possible to determine the effect of the adjustments.

3.17 ASTM G48-11

The G48-11 (Standard Test Methods for Pitting and Crevice Corrosion Resistance of Stainless Steels and Related Alloys by Use of Ferric Chloride Solution) test was used to determine the resistance of stainless steels and related alloys to the development of pitting and crevice corrosion. In this way, the alloys can be ranked in order of increasing resistance to pitting and crevice corrosion. The specimens were cut to a size of 25 x 50 mm^2. Then the test "Method A - ferric chloride pitting test" was selected. 600 ml of the ferric chloride test solution was poured into the 1000 ml test beaker, and the specimens were properly placed in the beaker to avoid contact with the other specimens. In total, the samples were left in the solution at 22 °C for 72 hours. The samples were rinsed with water and then examined under the light microscope. Subsequently, the elements of the samples were analysed with FESEM/EDS.

4 RESULTS

4.1 The 1st test run

4.1.1 As-cleaned samples

The samples were visually inspected before executing the salt spray test in order to determine which sample had been best irradiated with the laser. As can be seen from figure 21 variables “D", "B" and "F" had the biggest influence. This is also observed from the main effects plot (Fig. 22), where “VI” stands for the cleanness value (“Visual Inspection”) estimated with the method given in chapter 3.8. Here, it was evaluated how well the oxidation layer was cleaned, not how the laser cleaning affected the corrosion properties.

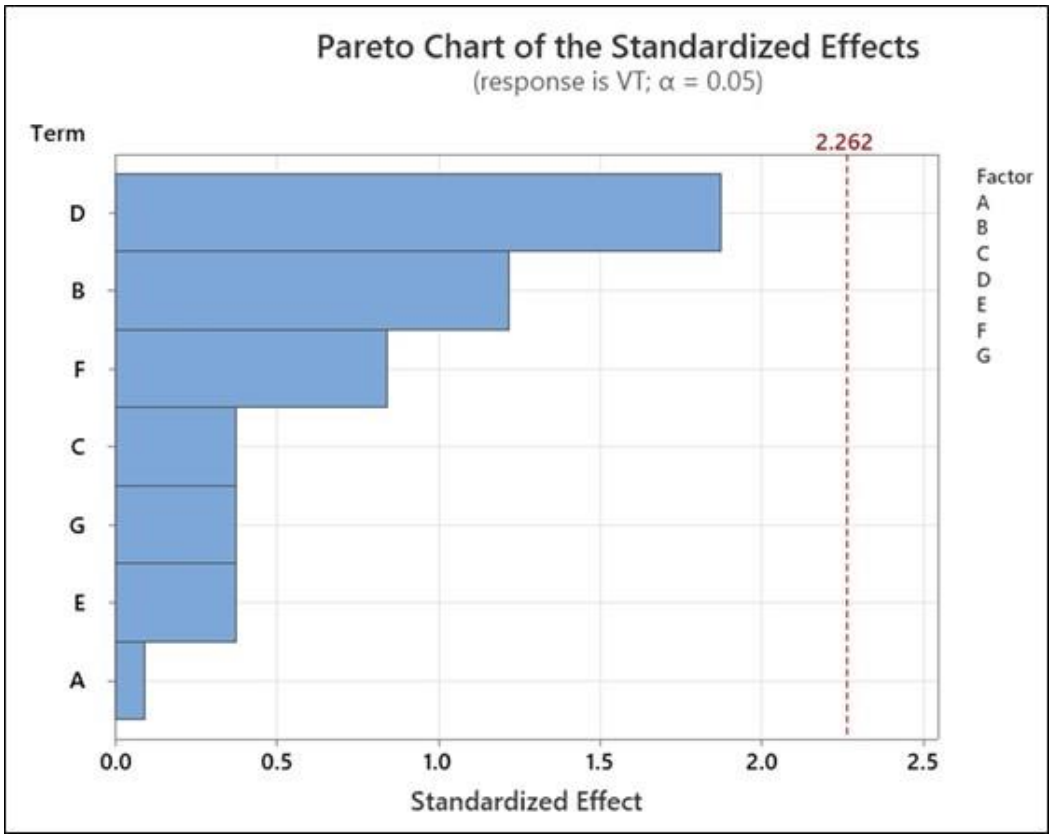

Figure 21 The 1st run Pareto chart before salt spray tests

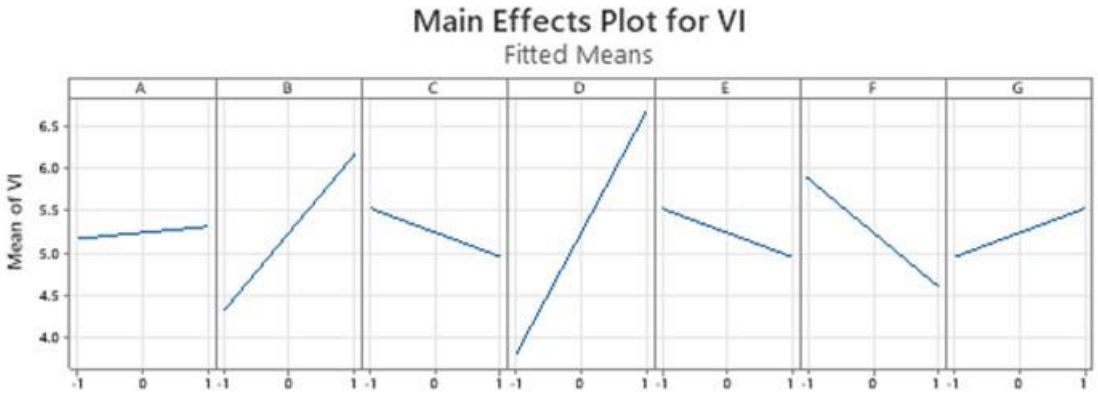

Figure 22 The 1st run main effects plot

4.1.2 Salt spray test

After the samples had been treated with salt spray, they were graded from 1 for the least corrosion resistance to 10 for no corrosion as defined in chapter 3.8. The parameters "C", "B" and "D" had now the biggest influence on corrosion resistance. The best result could be achieved when the sample was cleaned with a high “B” at a lower “C” and a higher “D”, see figures 23 and 24. The evaluation followed the same principle as given in chapter 3.8.

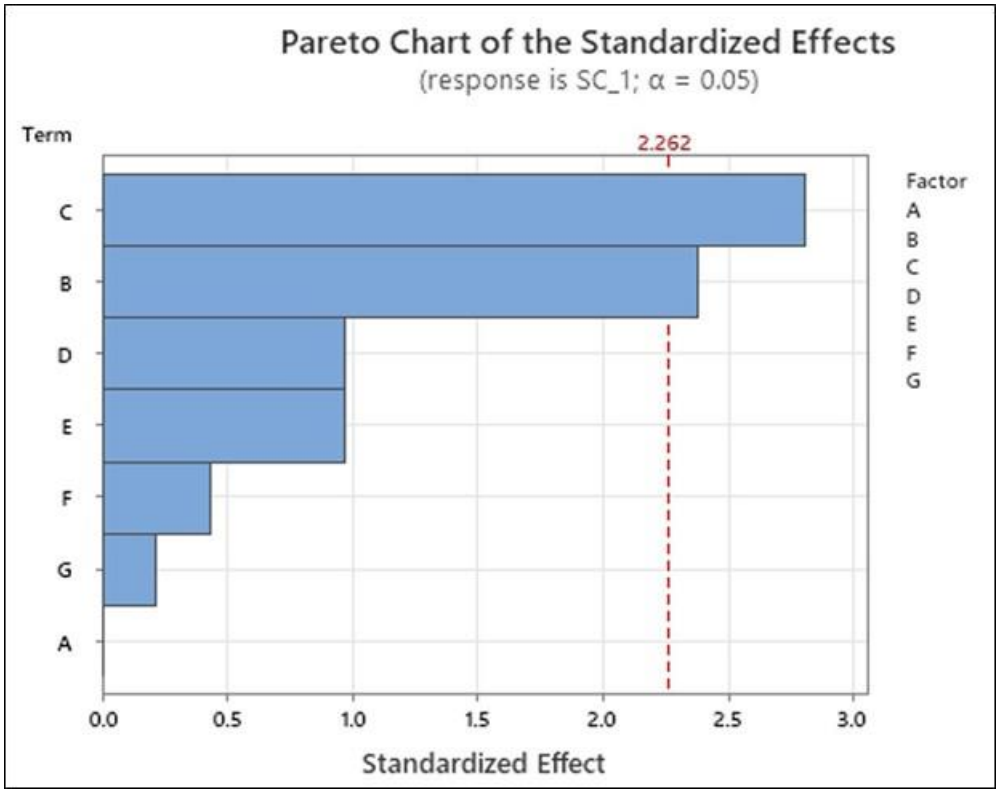

Figure 23 The 1st run Pareto chart after salt spray test

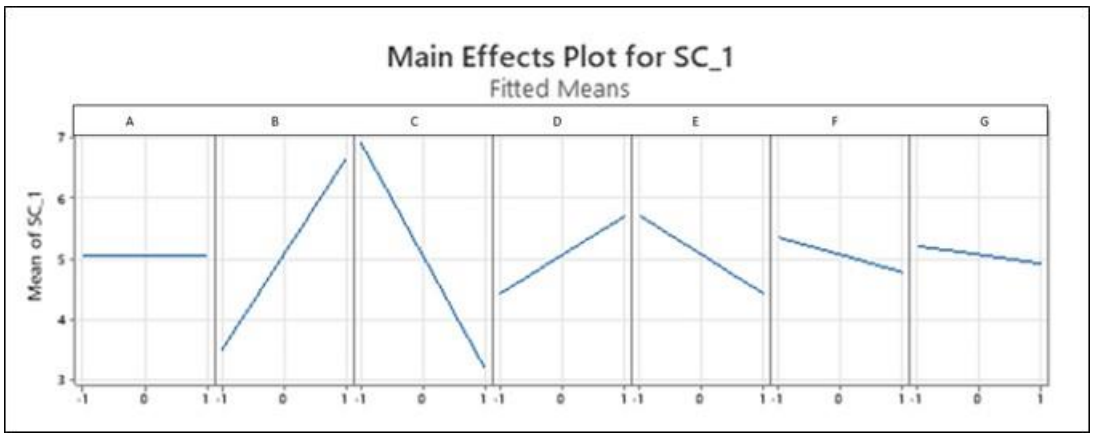

Figure 24 The 1st run main effects plot

4.1.3 Avesta Cell experiments

By analysing the Avesta cell experiments, three important points can be read from the diagram, namely E_{corr}, E_{rep} and E_{pit}. From the diagram, i_{corr} value can also be determined and corrosion rate (CR) is possible to calculate afterwards. The resulting cyclic polarization curves are represented in figures 25 - 29. These values will be analyzed in more details in the "Discussion" section.

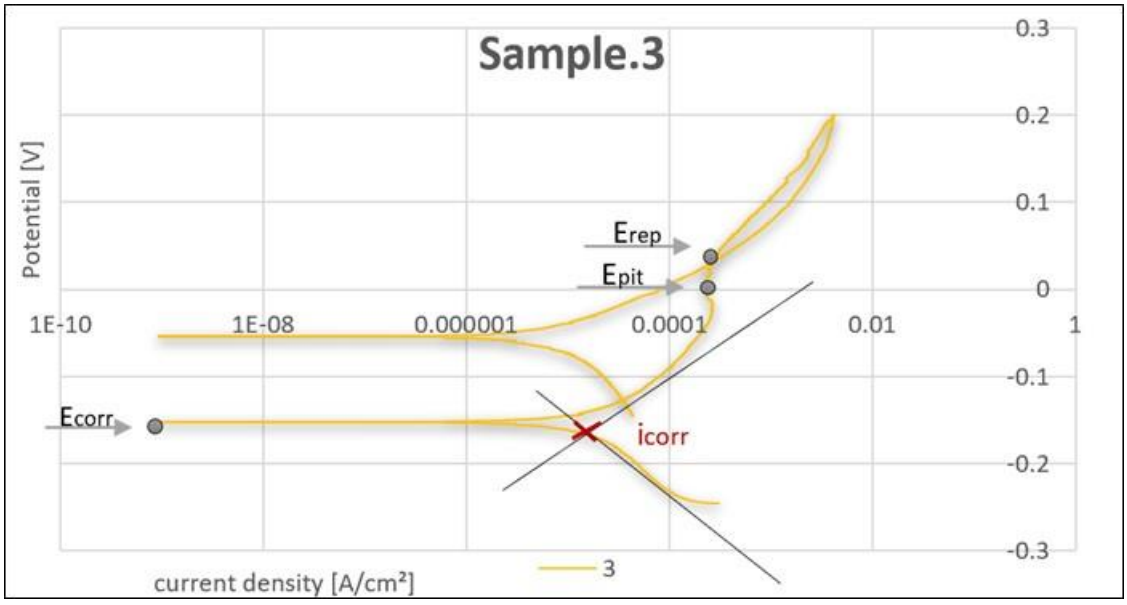

Figure 25 Cyclic polarization curve for the 1st run of Sample 1.3

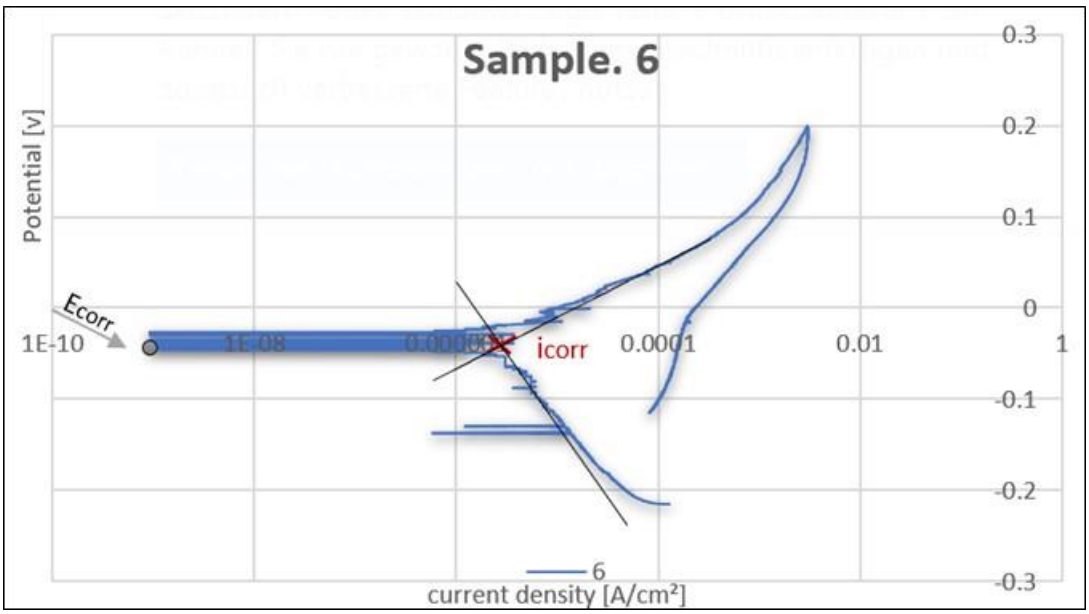

Figure 26 Cyclic polarization curve for the 1st run of Sample 1.6

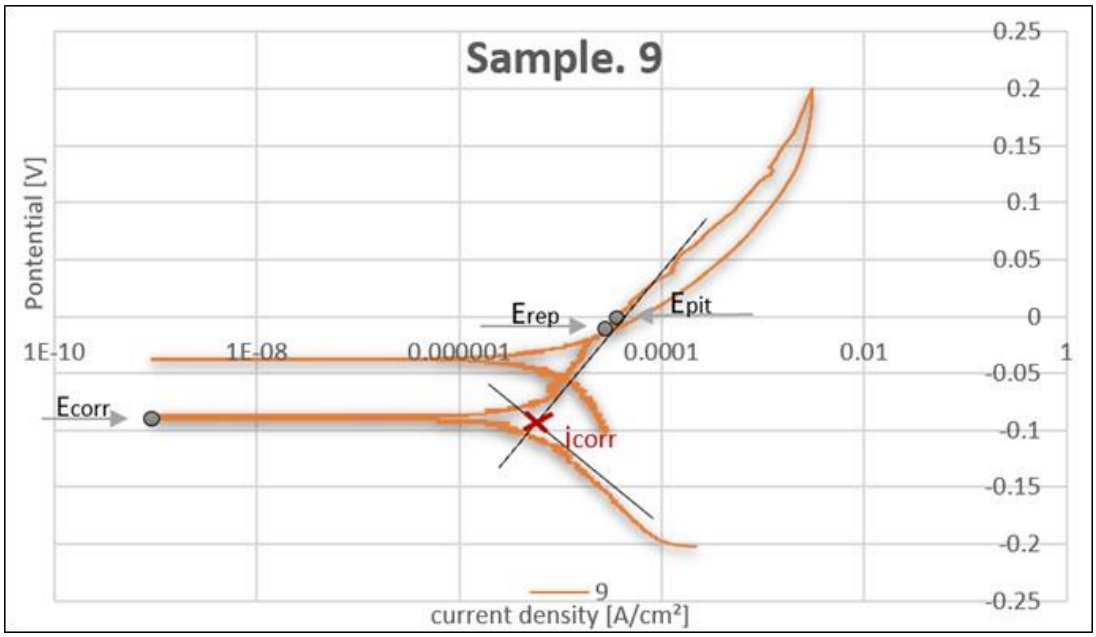

Figure 27 Cyclic polarization curve for the 1st run of Sample 1.9

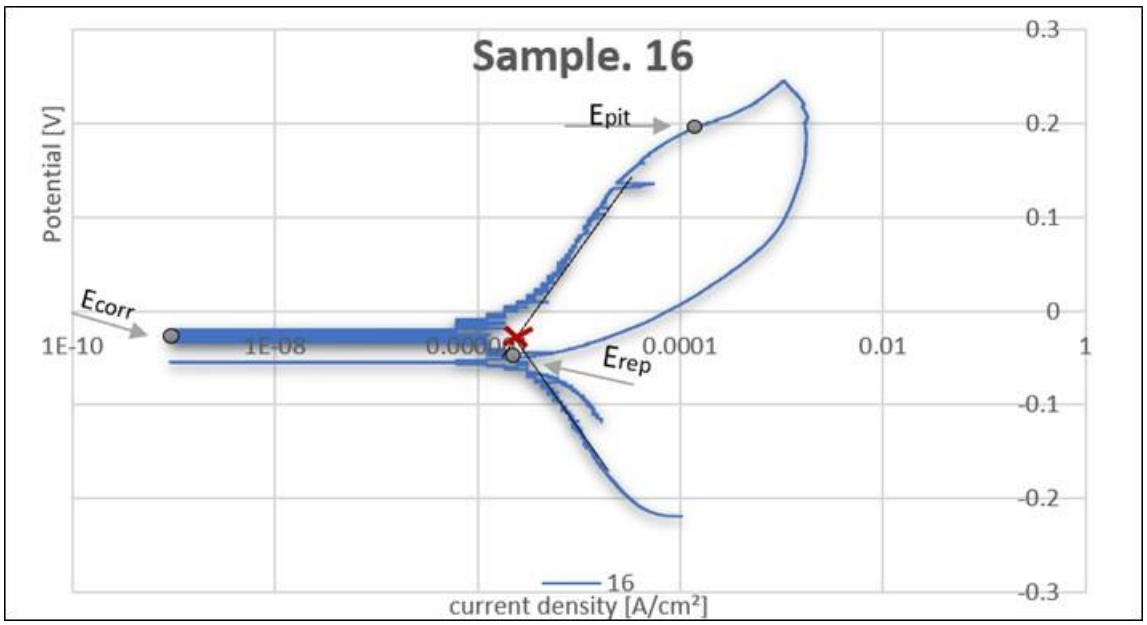

Figure 28 Cyclic polarization curve for the 1st run of Sample 1.16

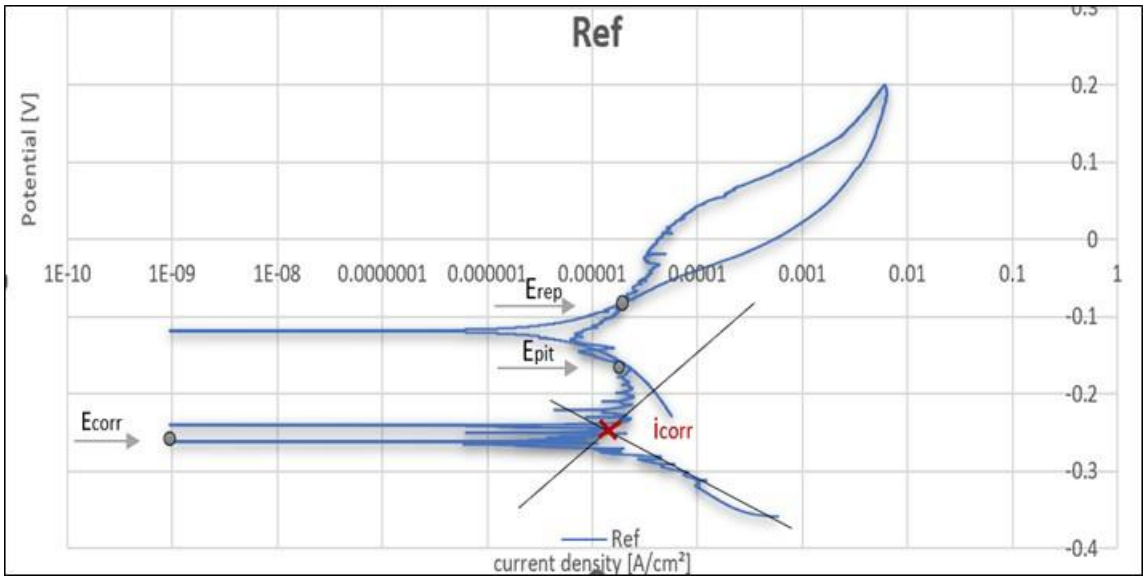

Figure 29 Cyclic polarization curve for the 1st run of REF sample

Corrosion rate (CR) can be calculated from the results using the following equation:

$$CR\ \left[\frac{\text{mm}}{\text{year}}\right] = \frac{\left(3.2710^{-3}\ \times\ {}_{i_{corr}}E_w\ \right)}{\rho}\ (1)$$

I_{corr} $[\frac{\mu A}{cm^2}]$ is the corrosion current

E_w [g] is the weight of the sample

ρ $[\frac{g}{cm^3}]$ is the density of the sample

CR $[\frac{mm}{year}]$ is the corrosion rate

4.1.4 EDS-analyses

Since the oxidation layer was cleaned during the first test run with a 20-watt and a 60-watt laser machine, the effect could best be analysed using the EDS-analysis. There is up to 60 % less Mn in the alloys at 60 watts than in the 20-watt samples. Oxygen is also 40 % less present, and the same applies to Si, see figures 30 - 33 and tables 6 - 9.

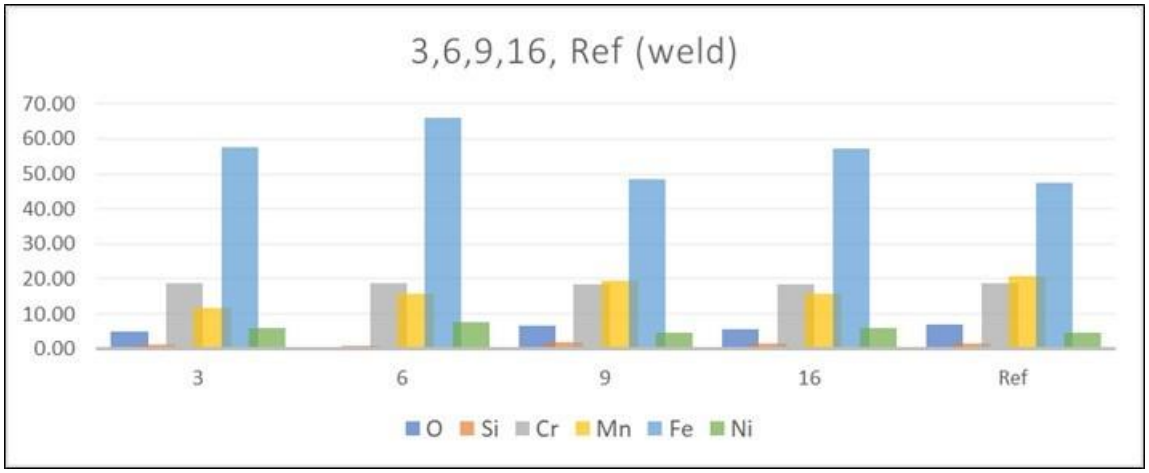

Figure 30 1st run, elements of the samples with 20 Watts, next to the weld.

Table 6 1st run, elements of the samples with 20 Watts, next to the weld.

Samples	O [%]	Si [%]	Cr [%]	Mn [%]	Fe [%]	Ni [%]
1.3	4.91	1.36	18.68	11.64	57.53	5.89
1.6		1.02	18.81	15.64	66.07	7.61
1.9	6.64	1.95	18.29	19.47	48.50	4.60
1.16	5.77	1.44	18.59	15.58	57.37	6.03
Ref	6.92	1.51	18.75	20.79	47.54	4.51

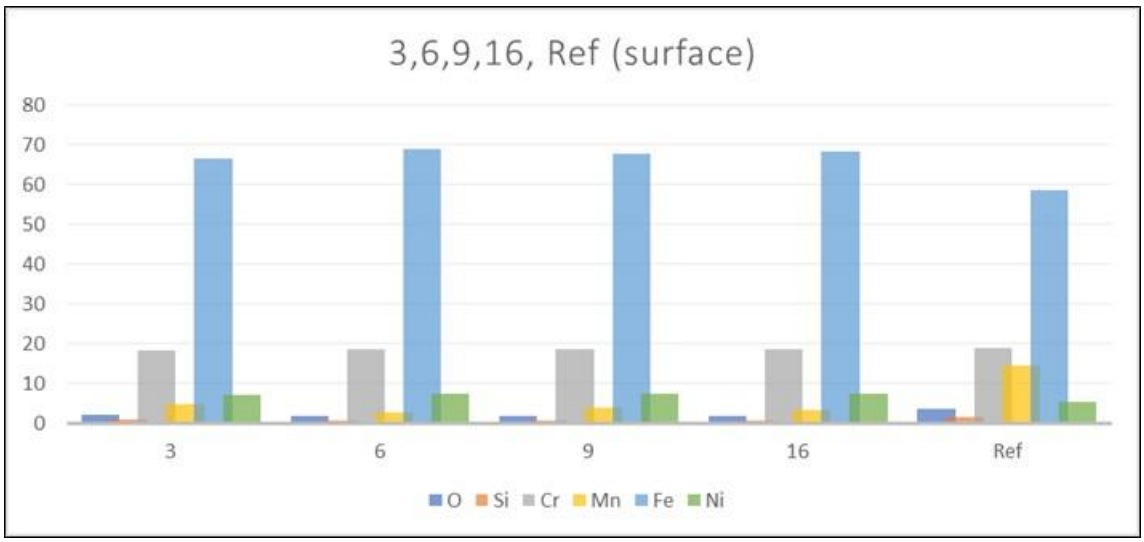

Figure 31 The 1st run elements of the samples with 20-watt, surface

Table 7 The 1st run elements of the samples with 20-watt, surface

Samples	O [%]	Si [%]	Cr [%]	Mn [%]	Fe [%]	Ni [%]
1.3	2.16	0.80	18.39	4.84	66.60	7.22
1.6	1.67	0.58	18.72	2.60	69.03	7.41
1.9	1.91	0.69	18.56	3.72	67.81	7.31
1.16	1.79	0.63	18.64	3.16	68.42	7.36
Ref	3.57	1.47	18.89	14.37	58.64	5.43

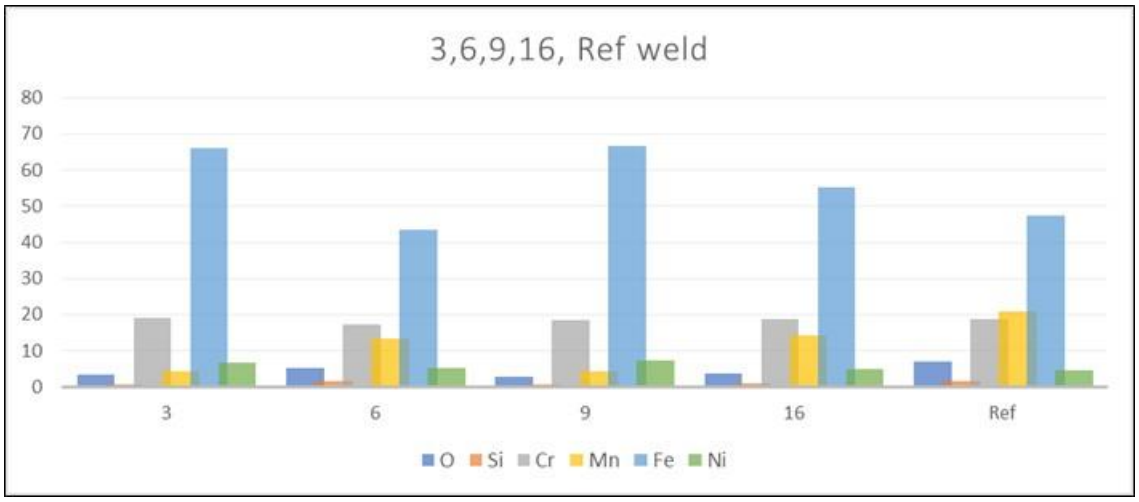

Figure 32 The 1st run elements of the samples with 60-watt, next to the weld

Table 8 The 1st run elements of the samples with 60-watt, next to the weld

Samples	O [%]	Si[%]	Cr[%]	Mn[%]	Fe[%]	Ni[%]
1.3	3.51	0.67	19.19	4.47	65.92	6.6
1.6	5.19	1.47	17.32	13.32	43.54	5.22
1.9	2.67	0.58	18.44	4.24	66.79	7.27
1.16	3.79	1.13	18.70	14.31	55.37	5.06
Ref	6.92	1.51	18.75	20.79	47.54	4.51

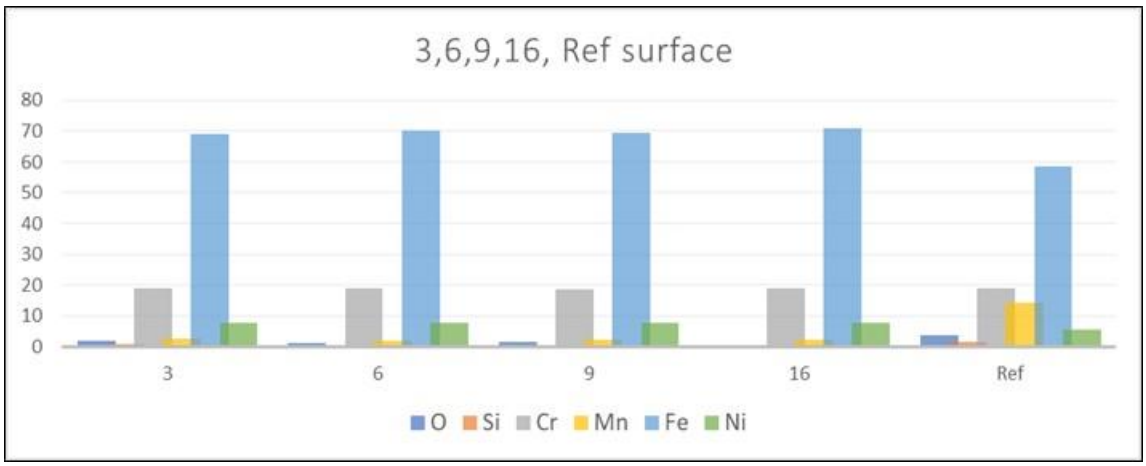

Figure 33 The 1st run elements of the samples with 60-watt, surface

Table 9 The 1st run elements of the samples with 60-watt, surface

Samples	O [%]	Si [%]	Cr [%]	Mn [%]	Fe [%]	Ni [%]
1.3	1.83	0.64	18.82	2.57	69.08	7.62
1.6	1.28	0.51	18.98	1.96	70.31	7.60
1.9	1.54	0.51	18.42	2.14	69.54	7.52
1.16		0.49	18.88	2.18	70.85	7.77
Ref		1.47	18.89	14.37	58.64	5.43

4.2 The 2nd run

From the second experiment onwards, the root side of each sample was also cleaned with the laser i.e., " Root side (bottom-part)", as no root shielding gas was used during welding. The use of laser cleaning could therefore replace such a gas protection in the future.

4.2.1 After Salt spray test

After the samples were treated with salt spray, they were rated from 1 for the least corrosion resistance to 10 for no corrosion, the evaluation of the samples was carried out as in chapter 3.8 It can be seen that the parameters "C", "D" and "E" have the greatest influence on the corrosion resistance. For the best result in this test run, see figure 34 and 35.

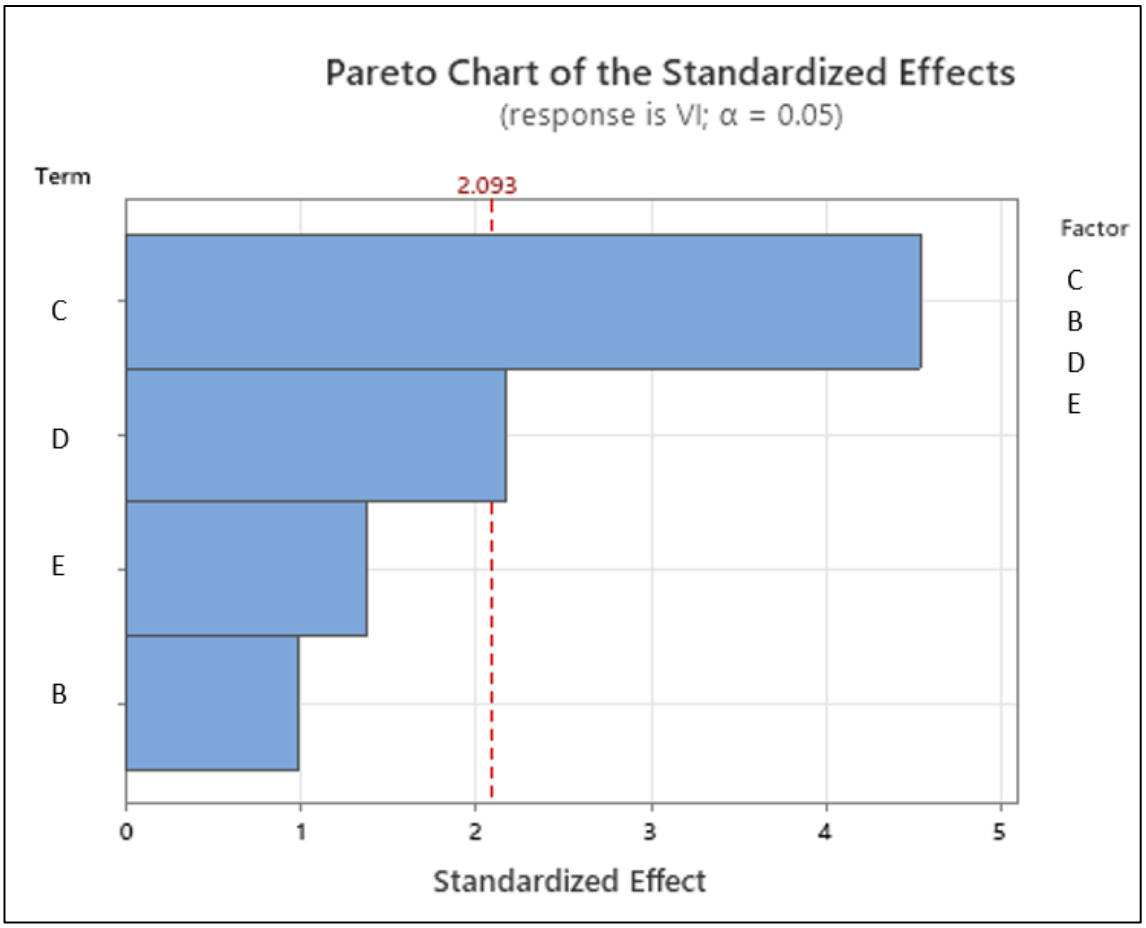

Figure 34 The 2nd run Pareto Chart after salt spray

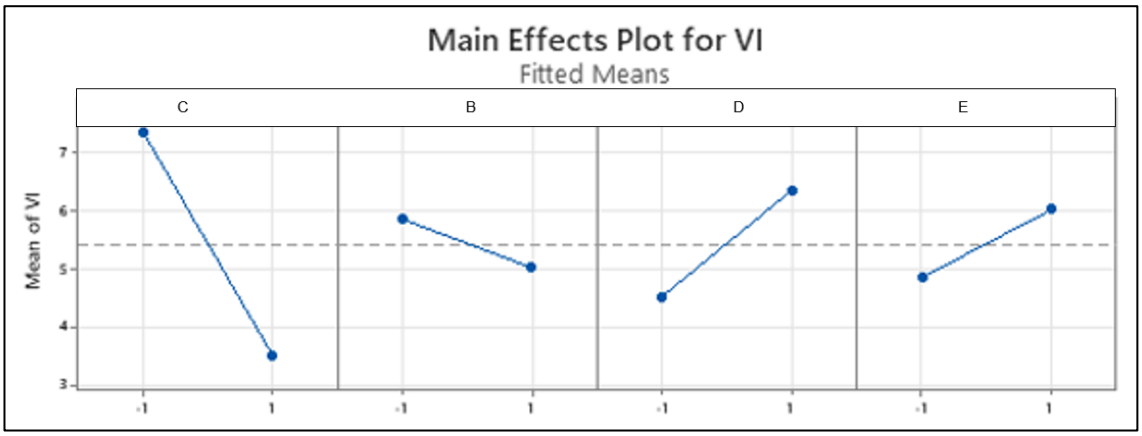

Figure 35 The 2nd run main effects plots

4.2.2 EDS-analysis

After the oxidation layer was removed with the laser, the element composition on the surface also changed. This could be determined by EDS-analysis, see Fig. 36, 37 and 38.

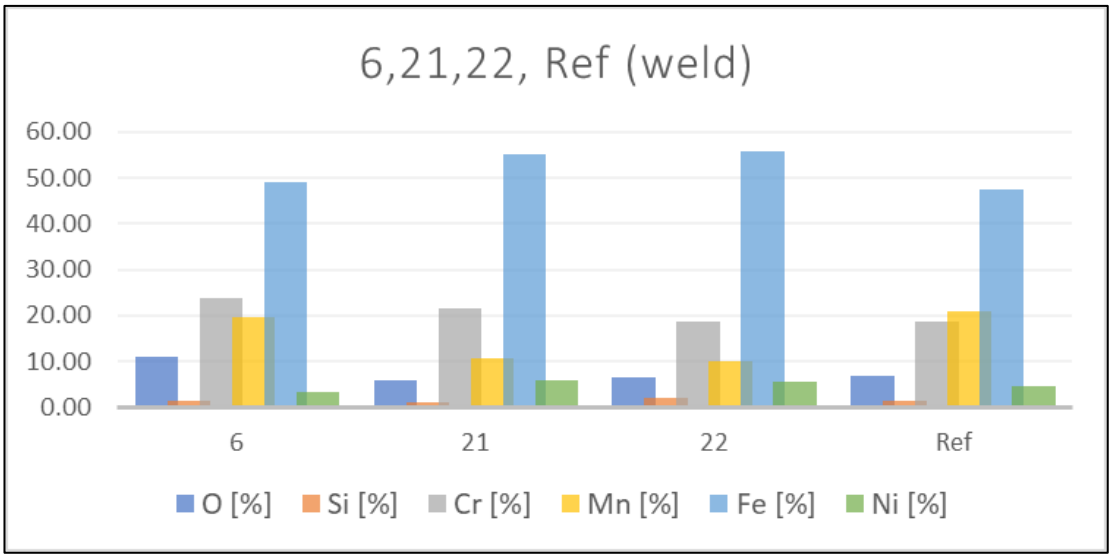

Figure 36 The 2nd run Elements of the samples with 20-watt, next to the weld

Table 10 The 2nd run Elements of the samples with 20 -watt, next to the weld

Samples	O [%]	Si [%]	Cr [%]	Mn [%]	Fe [%]	Ni [%]
2.6	11.17	1.34	23.69	19.54	49.00	3.35
2.21	5.92	1.07	21.55	10.59	55.05	5.83
2.22	6.92	2.06	18.84	9.94	55.60	5.59
Ref	7.67	1.16	22.26	13.57	53.03	5.00

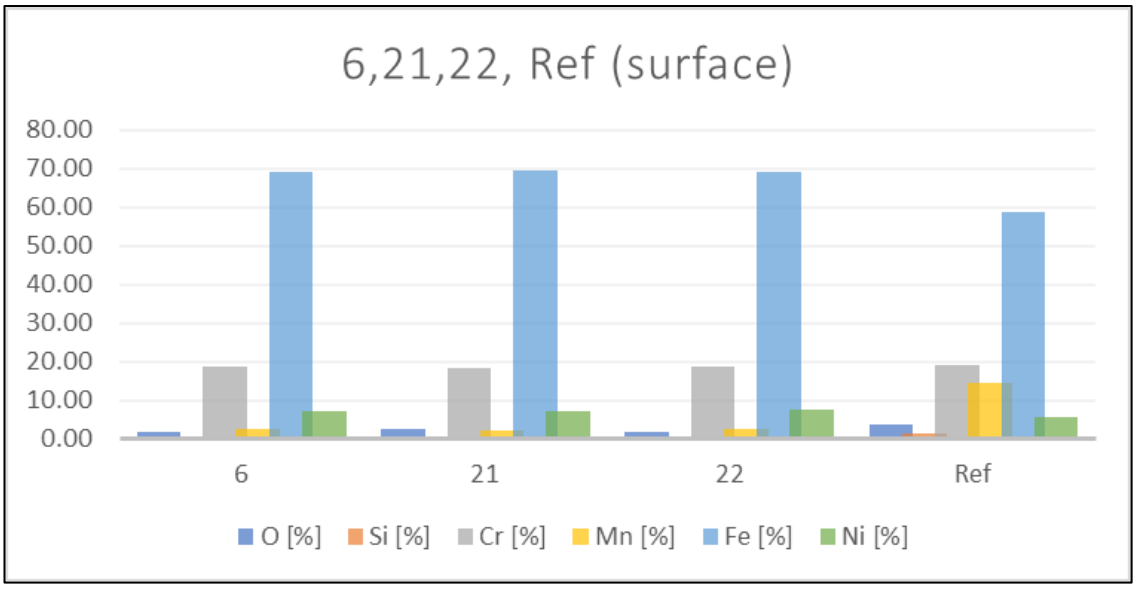

Figure 37 The 2nd run Elements of the samples with 20-watt, surface

Table 11 The 2nd run Elements of the samples with 20-watt, surface

Samples	O [%]	Si [%]	Cr [%]	Mn [%]	Fe [%]	Ni [%]
2.6	1.59	0.52	18.69	2.66	69.33	7.22
2.21	2.33	0.50	18.30	2.05	69.58	7.25
2.22	1.65	0.60	18.68	2.43	69.27	7.39
Ref	3.57	1.47	18.89	14.37	58.64	5.43

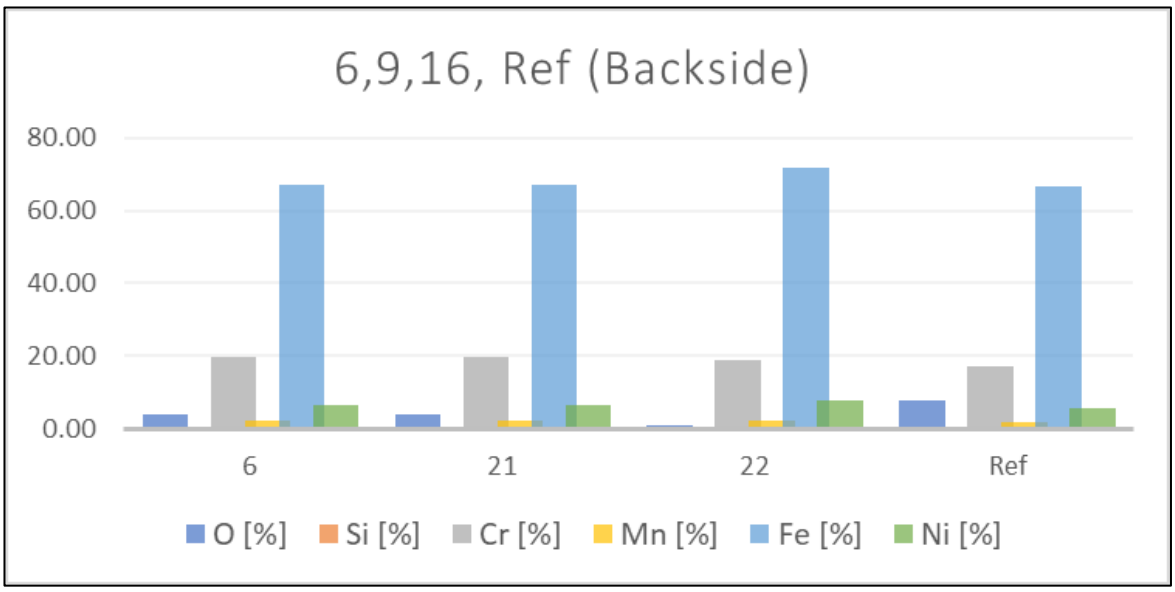

Figure 38 The 2nd run Elements of the samples with 20-watt, Root side

Table 12 The 2nd run Elements of the samples with 20-watt, Root side

Samples	O [%]	Si [%]	Cr [%]	Mn [%]	Fe [%]	Ni [%]
2.6	3.97	0.55	19.76	2.25	67.07	6.41
2.21	3.50	0.61	19.46	2.16	67.49	6.82
2.22	1.06	0.48	18.76	2.15	71.69	7.74
Ref	7.80	0.78	17.01	1.81	66.57	5.81

4.2.3 Ferric chloride test

It can be seen in the figure 41, that small to medium pitting corrosion predominates in the reference sample next to and on the weld. On the root side most of the pitting corrosion (medium holes) is on the oxidation layer. In sample 6, there is only small pitting corrosion next to the weld and one large pitting corrosion, but on the weld the pitting corrosion is predominant, on the root side the small pitting corrosion is increased. In specimen 21, there is only pitting on the weld and medium pitting on the root side. In specimen 22, there is very little pitting next to the weld seam, increased pitting occurs on the weld seam, but there is no pitting on the reverse side.

Sample	Frontside	Root side
Ref	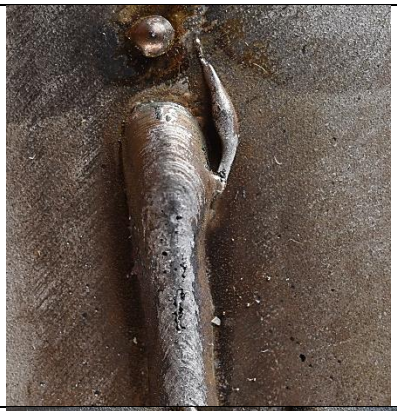	
2.6	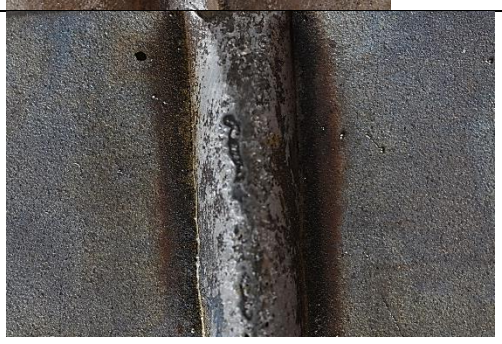	

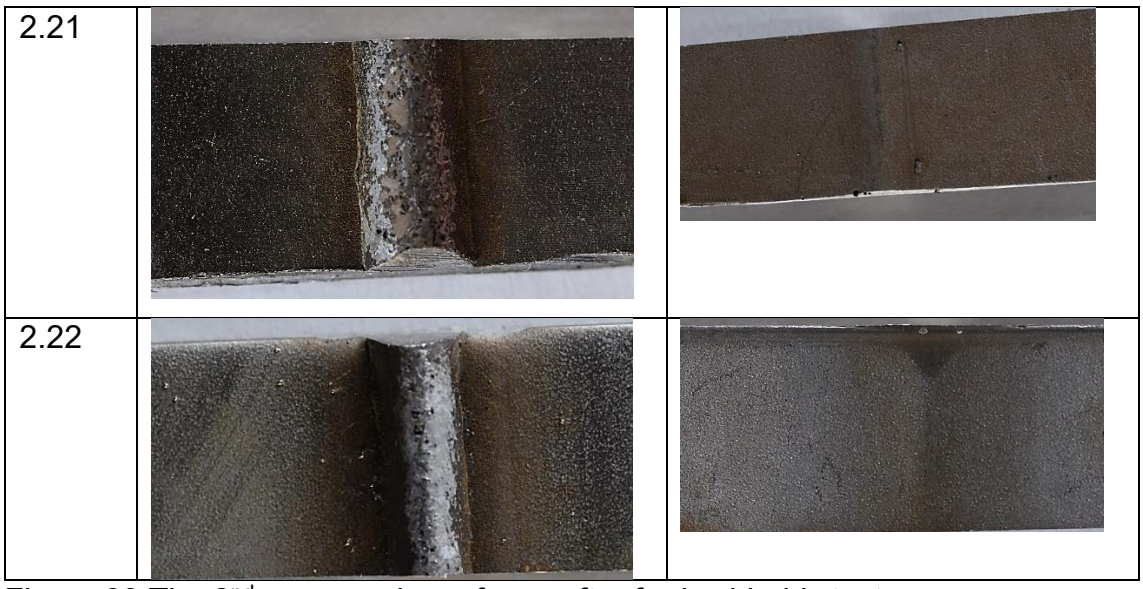

Figure 39 The 2nd run sample surfaces after ferric chloride test

4.2.4 EDS-analysis of the ferric chloride sample

For the samples of the 2nd run which were before treated with the ferric chloride pitting test, the effect of the test could be analysed with the EDS. If the amount of the Elements of the sample had changed, see figure 39 and 40.

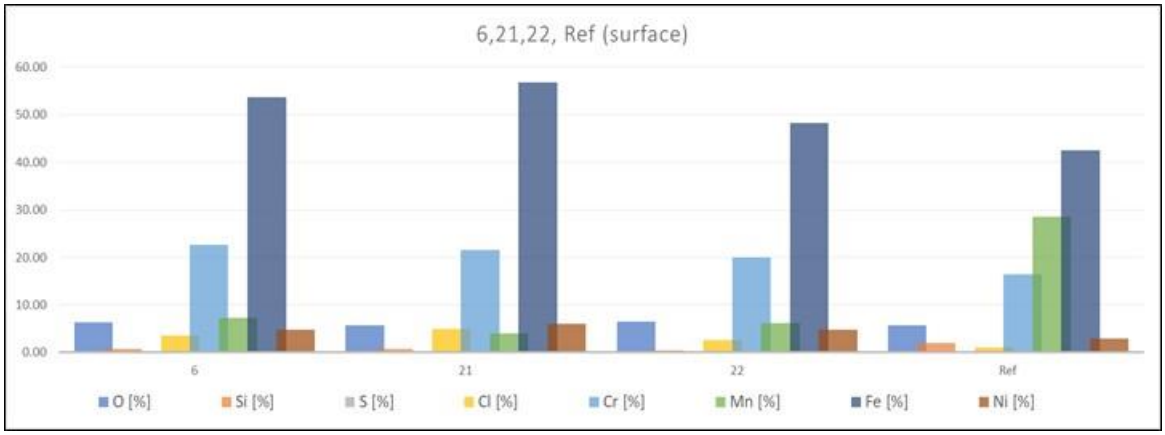

Figure 40 The 2nd run with $FeCl_3$ elements of the samples with 20-watt, surface

Table 13 The 2nd run with $FeCl_3$ elements of the samples with 20-watt, surface

Samples	O [%]	Si [%]	S [%]	Cl [%]	Cr [%]	Mn [%]	Fe [%]	Ni [%]
2.6	6.28	0.68	0.26	3.59	22.56	7.28	53.65	4.72
2.21	5.70	0.69	0.30	4.93	21.50	3.95	56.71	6.05
2.22	6.52	0.51		2.57	19.97	6.14	48.27	4.80
Ref	5.69	1.94	0.12	1.13	16.38	28.53	42.42	2.89

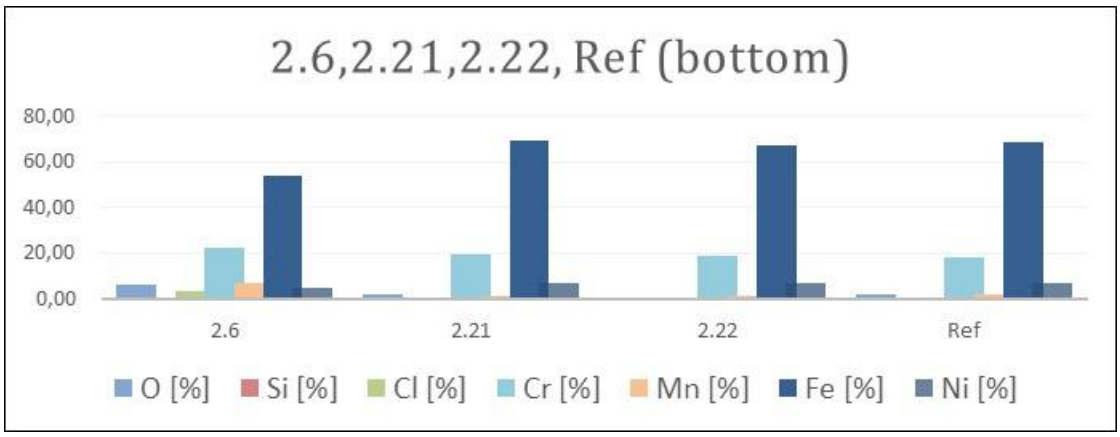

Figure 41 The 2nd run with $FeCl_3$ elements of the samples with 20-watt, Root side

Table 14 The 2nd run with $FeCl_3$ elements of the samples with 20-watt, Root side

Samples	O [%]	Si [%]	Cl [%]	Cr [%]	Mn [%]	Fe [%]	Ni [%]
2.6	6.28	0.68	3.59	22.56	7.28	53.65	4.72
2.21	2.07	0.53	0.35	19.80	1.72	69.33	7.07
2.22	0.75	0.42	0.29	18.71	1.69	67.33	6.80
Ref	1.99	0.54	0.94	18.27	1.90	68.74	7.27

4.3 The 3rd test run

For the third experiment onwards, the root side of each sample was also cleaned with the laser "back side (lower part)", since no root shielding gas was used during welding. The use of laser cleaning could therefore replace such gas protection.

4.3.1 After Salt spray test

After the samples had been treated with salt spray test, the evaluation of the samples was carried out as described in chapter 3.8. As a result, Figures 42 and 43 were obtained, showing how the laser machine settings "C" and "D" affect the corrosion properties of the specimens. The values for "C" and "D" should be low.

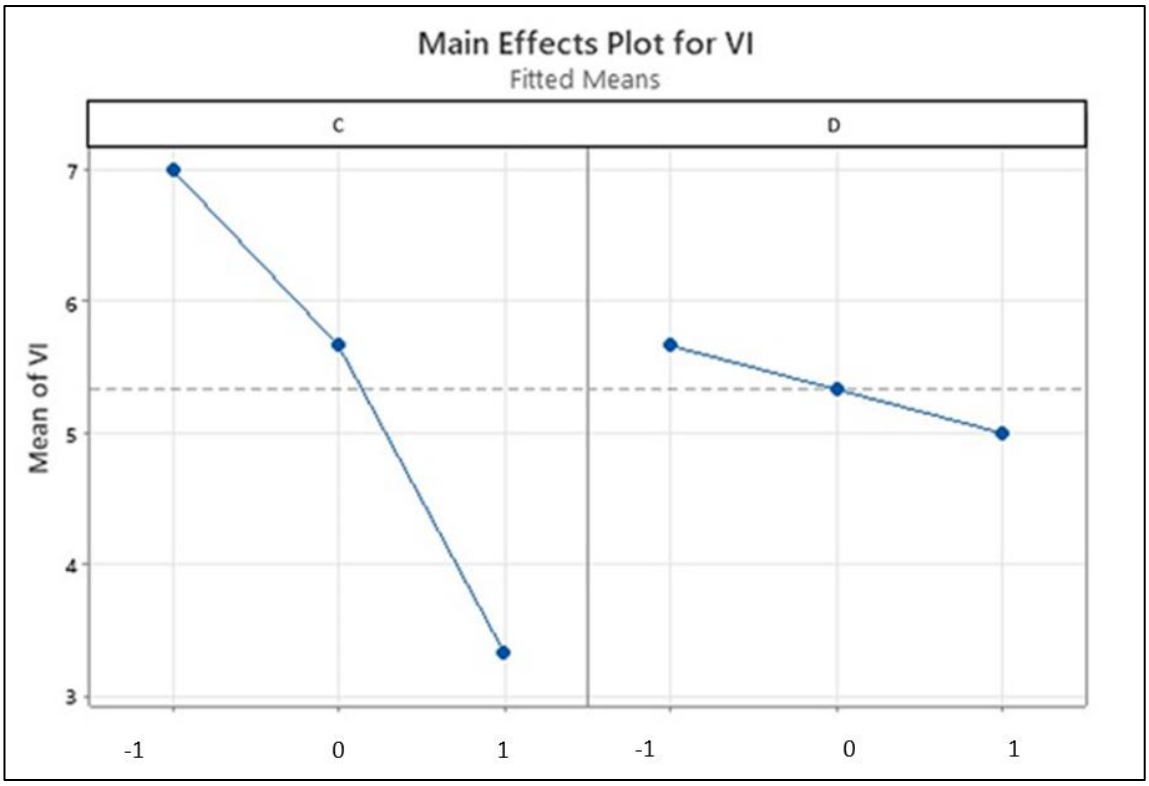

Figure 42 The 3rd run main effects plots

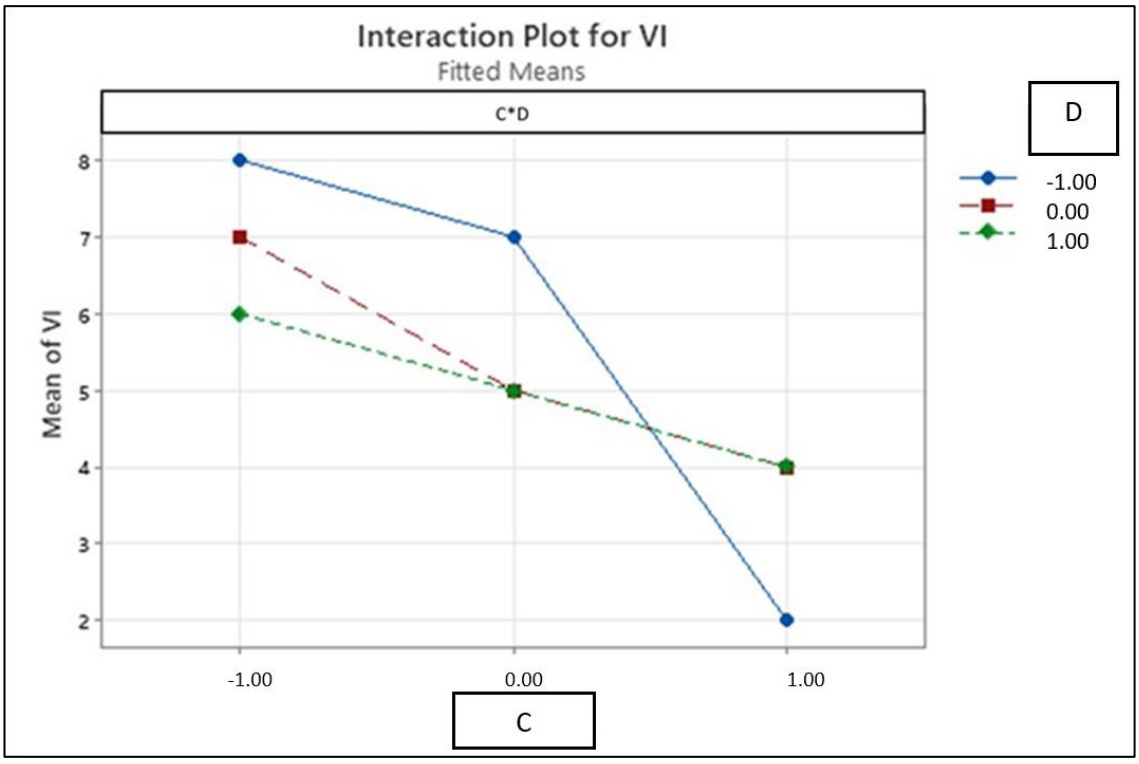

Figure 43 Interaction plots between C and D

4.3.2 EDS – analysis

After the oxidation layer of the weld seam was removed with the laser, both on the "frontside" and "bottom side", the element composition on the surface also changed. This could be determined by EDS-analysis, see Fig.44, 45 and 46.

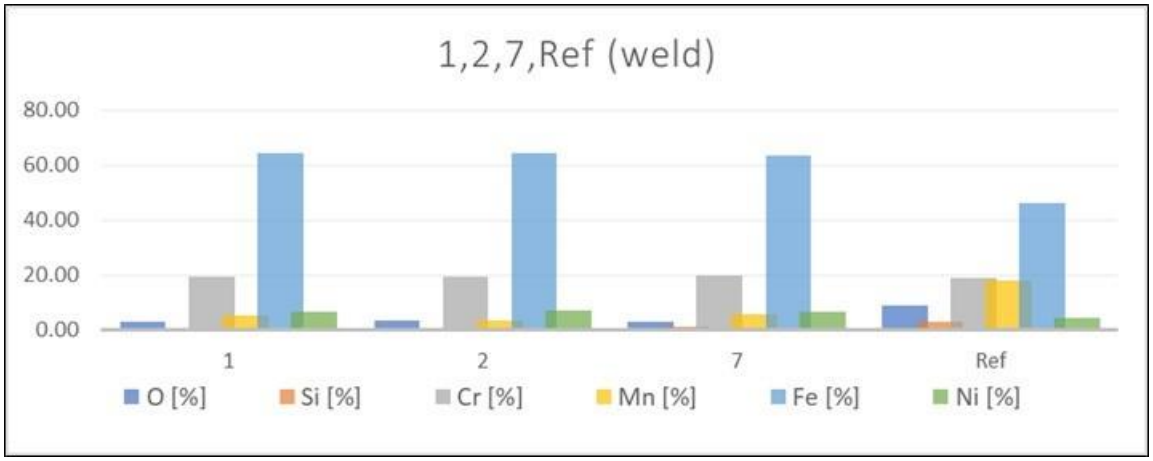

Figure 44 The 3rd run elements of the samples with 20 watts, next to the weld

Table 15 The 3rd run elements of the samples with 20 watts, next to the weld

Samples	O [%]	Si [%]	Cr [%]	Mn [%]	Fe [%]	Ni [%]
3.1	3.25	0.97	19.44	5.47	64.36	6.51
3.2	3.56	0.75	19.20	3.58	64.53	7.35
3.7	2.98	1.12	19.87	5.69	63.51	6.78
Ref	8.88	3.09	18.87	17.92	46.11	4.48

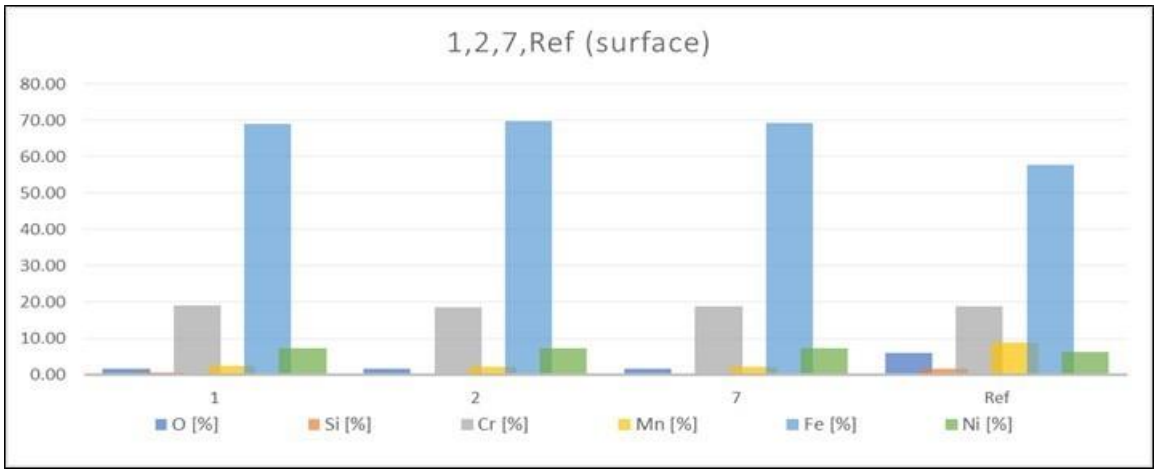

Figure 45 The 3rd run elements of the samples with 20-watt, surface

Table 16 The 3rd run elements of the samples with 20-watt, surface

Samples	O [%]	Si [%]	Cr [%]	Mn [%]	Fe [%]	Ni [%]
3.1	1.56	0.59	19.12	2.53	68.96	7.24
3.2	1.70	0.48	18.68	2.09	69.66	7.41
3.7	1.63	0.53	18.90	2.31	69.31	7.32
Ref	5.99	1.72	18.80	8.93	57.64	6.24

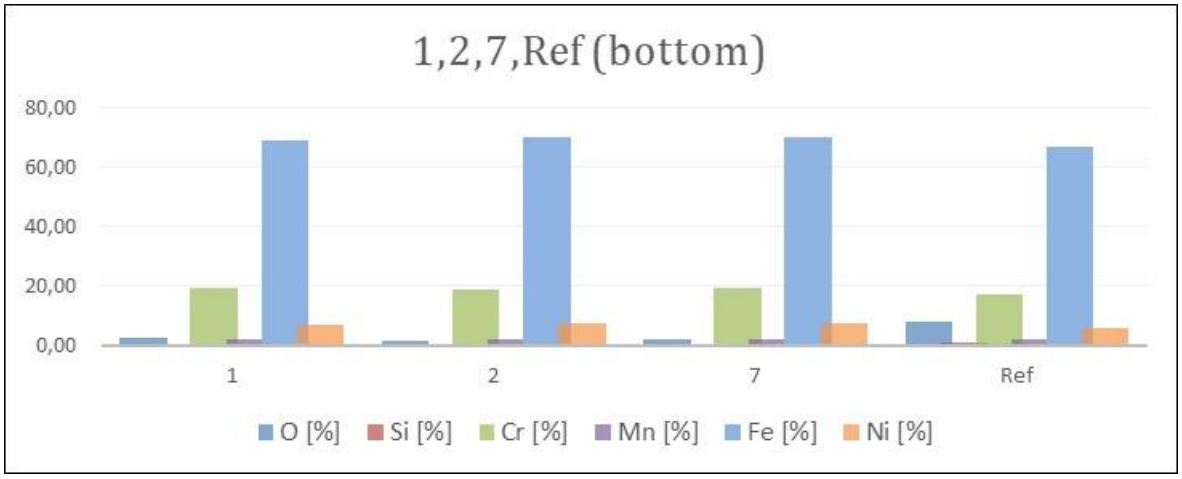

Figure 46 The 3rd run elements of the samples with 20-watt, Root side

Table 17 The 3rd run elements of the samples with 20-watt, Root side

Samples	O [%]	Si [%]	Cr [%]	Mn [%]	Fe [%]	Ni [%]
3.1	2.65	0.58	19.09	1.90	68.92	6.83
3.2	1.25	0.46	18.84	2.20	70.01	7.26
3.7	1.79	0.54	19.17	2.00	70.04	7.40
Ref	7.80	0.78	17.01	1.81	66.57	5.81

4.3.3 Ferric chloride test

All samples were welded with the same settings, but one reference from each batch was analysed. In the figure 49, the reference has an extremely large amount of pitting on the weld and large, deep pitting next to it, with deep, large pitting next to the oxide layer. Sample 1 exhibits only a few deep pitting spots on the weld, but no pitting on the root side. Sample 2 exhibits more pitting on the weld, but no pitting on the root side. The seventh specimen shows only a little pitting on the weld, with three small pitting spots on the root side.

Sample	Frontside	Root side
Ref		
3.1		
3.2		
3.7		

Figure 47 The 3rd run sample surfaces after ferric chloride test

4.3.4 EDS-analysis of the ferric chloride sample

For the samples of the 3rd run which were after treated with the ferric chloride pitting test, the effect of the test could be analysed with the EDS. If the amount of the elements of the sample had changed, see figure 39 and 40.

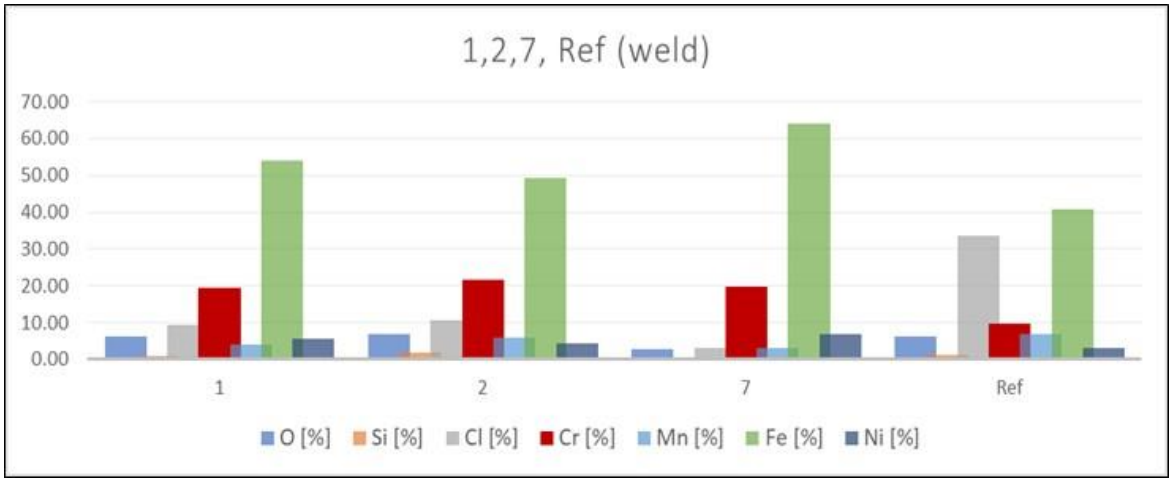

Figure 48 The 3rd run with $FeCl_3$ elements of the samples with 20 watts, next to the surface

Table 18 The 3rd run with $FeCl_3$ elements of the samples with 20 watts, next to the surface

Samples	O [%]	Si [%]	Cl [%]	Cr [%]	Mn [%]	Fe [%]	Ni [%]
3.1	6.37	0.98	9.45	19.54	3.94	54.13	5.70
3.2	6.80	1.71	10.78	21.50	5.82	49.20	4.19
3.7	2.65	0.62	3.02	19.69	3.03	64.02	6.98
Ref	6.10	1.14	33.49	9.70	6.72	40.82	2.97

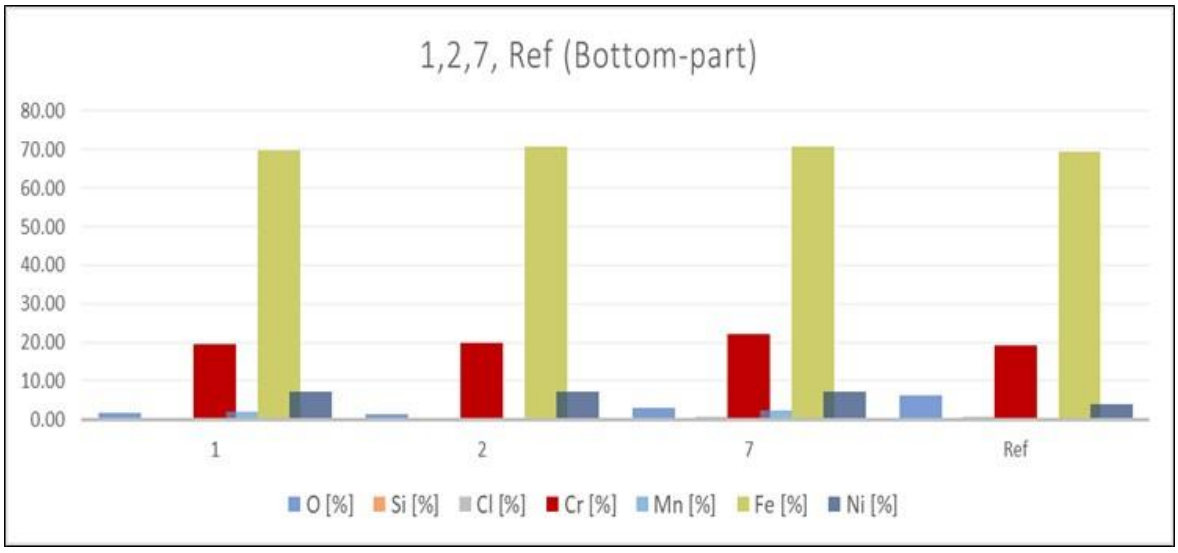

Figure 49 The 3rd run with $FeCl_3$ elements of the samples with 20-watt, Root side

Table 19 The 3rd run with $FeCl_3$ elements of the samples with 20-watt, Root side

Samples	O [%]	Si [%]	Cl [%]	Cr [%]	Mn [%]	Fe [%]	Ni [%]
3.1	6.37	0.98	9.45	19.54	3.94	54.13	5.70
3.2	6.80	1.71	10.78	21.50	5.82	49.20	4.19
3.7	2.65	0.62	3.02	19.69	3.03	64.02	6.98
Ref	5.27	1.10	33.40	9.70	6.72	40.82	2.97

4.4 The final testing

The 4th run was not really a test run like the other three runs before. This was an extra run. For this, sample 1.6 of the 1st run, which performed worst in the visual inspection after the salt spray test, was compared with sample 3.4, sample 4 of the 3rd run, which performed best in the visual inspection after the salt spray test. An extra for the sample 3.4 was laser cleaned again to remove the discoloration previously caused by the laser settings so that a nice visual laser cleaning can take place, this was referred to as Sample 3.4c.

All these extra samples were tested with the ferric chloride test. In the figure 52, specimen 1.6 shows pitting on the weld, only some very small pits are on the reverse side. Specimen 3.4 shows pitting on the weld seam, no pitting is visible on the root side, the same applies to specimen 3.4c.

It is very interesting that the pitting corrosion on the root side does not take place on the oxidation layer as assumed, but immediately afterwards. The same is true for the front side, but there is also large and deep pitting on the weld.

Sample	Frontside	Root side
1.6		
3.4		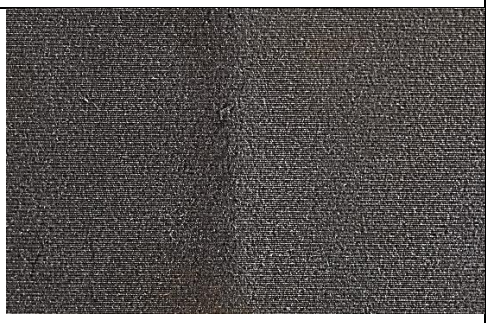
3.4c	Only the root side was especially post-cleaned with the laser (once again lasered with lower power), so that the discoloration (yellowish surface) was no longer present. Could be a disadvantage for the consumer because it does not meet the claims.	

Figure 50 The 4th run sample surfaces after ferric chloride test, 1.6 (duplicate sample from the 1st run), 3.4 (duplicate sample from the 3rd run) and 3.4 c (sample from 3rd run with extra lasering)

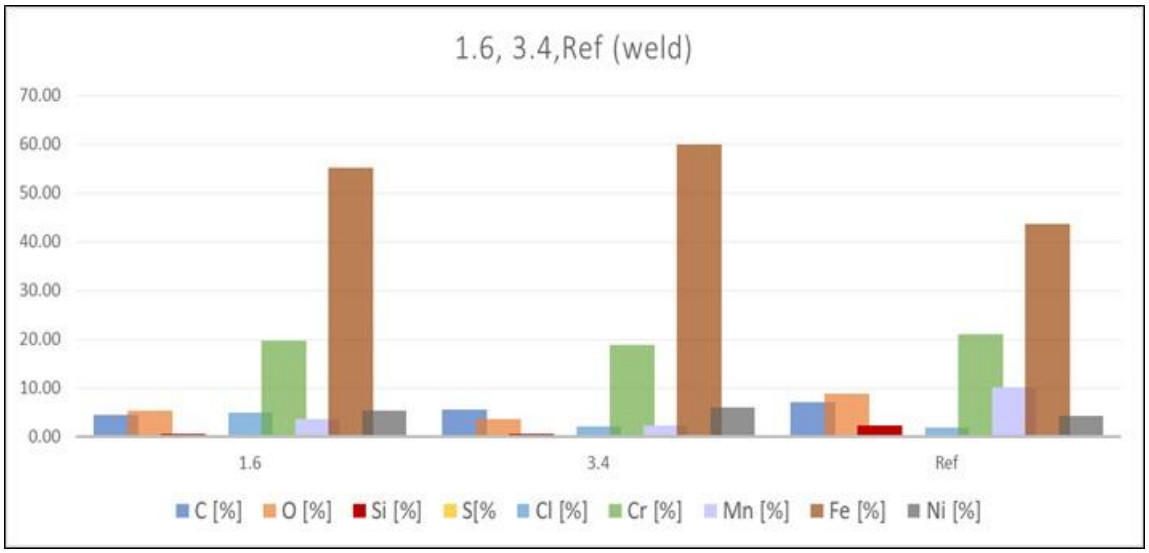

Figure 51 The 4th run after ferric chloride test, elements of the samples with 20-watt lasering, surface

Table 20 The 4th run after ferric chloride test, elements of the samples with 20-watt lasering, surface

Samples	C [%]	O [%]	Si [%]	S[%	Cl [%]	Cr [%]	Mn [%]	Fe [%]	Ni [%]
1.6	4.63	5.38	0.55	0.22	5.04	19.84	3.65	55.17	5.35
3.4	5.59	3.73	0.74	0.22	2.20	18.79	2.46	59.85	6.05
Ref	7.19	8.78	2.28	0.42	1.83	20.97	10.27	43.70	4.22

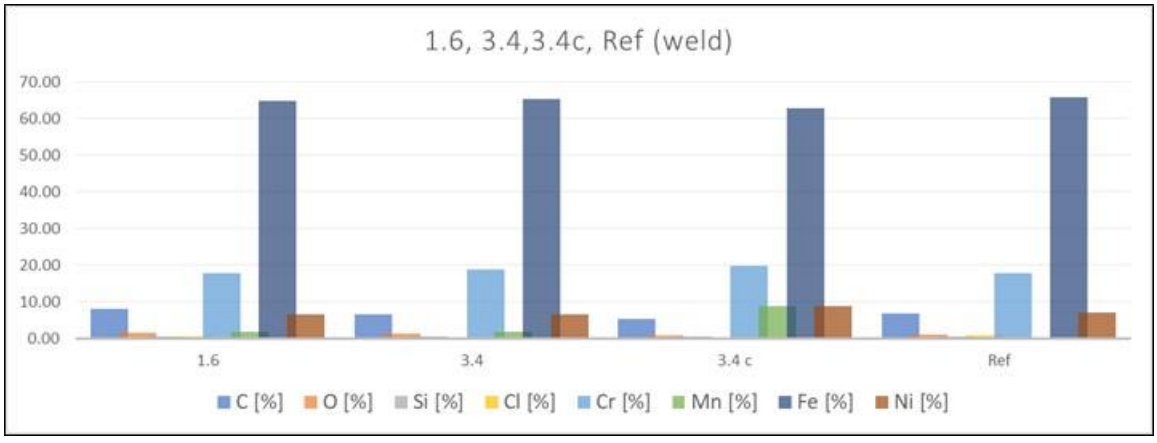

Figure 52 The 4th run after ferric chloride test, elements of the samples with 20-watt lasering, root side

Table 21 The 4th run after ferric chloride test, elements of the samples with 20-watt lasering, root side

Samples	C [%]	O [%]	Si [%]	Cl [%]	Cr [%]	Mn [%]	Fe [%]	Ni [%]
1.6	7.97	1.60	0.54	0.42	17.86	1.77	64.70	6.54
3.4	6.44	1.15	0.49		18.65	1.79	65.27	6.45
3.4c	5.21	0.68	0.61	0.38	19.64	8.65	62.70	8.76
Ref	6.88	1.07	0.55	0.85	17.87		65.75	6.92

5 DISCUSSION

5.1 Laser cleaning time

Depending on the settings, the time required for cleaning a 30 x 100 mm^2 weld area varied from 6 seconds to almost 6 minutes. Important factors that have a big influence on the cleaning time were: “G”, “C” and “F”. For the “F”, if the value 1 is used and for the “G”, one would be sufficient. However, it is possible that a yellowish discolouration may occur due to the laser cleaning, so it may be that a second pass with less “A” should be used, which should be an extra 15 seconds maximum for a sample size of 30 x 100 mm^2. However, with the last samples, it was noticeable that the time per sample was 10 % shorter with each pass, as the laser had already "warmed up". Therefore, it can be assumed that the laser cleaning over a longer period requires less time for the same size of sample cleaning.

5.2 Optimization

5.2.1 Cleaning

It makes sense to use a “D” in the range of 200 to 350x, but there is a suspicion that it is in this range that the discolouration of the surface occurs. So, there is still a need to vary the “D” to counteract the discolouration.

5.2.2 Topography

When the sample is cleaned with the optimal settings, which could be found out by the 3rd test run, the sample discolours on the front side as well as on the back side. The metal piece is discoloured on the front side as well as on the back side, as can be seen in the figure 53. Therefore, the same sample was cleaned with a second pass with the laser beam, but only 30 % of the “A” could be used. Thus, only the discoloured surface could be removed to meet the customer's expectations of this process.

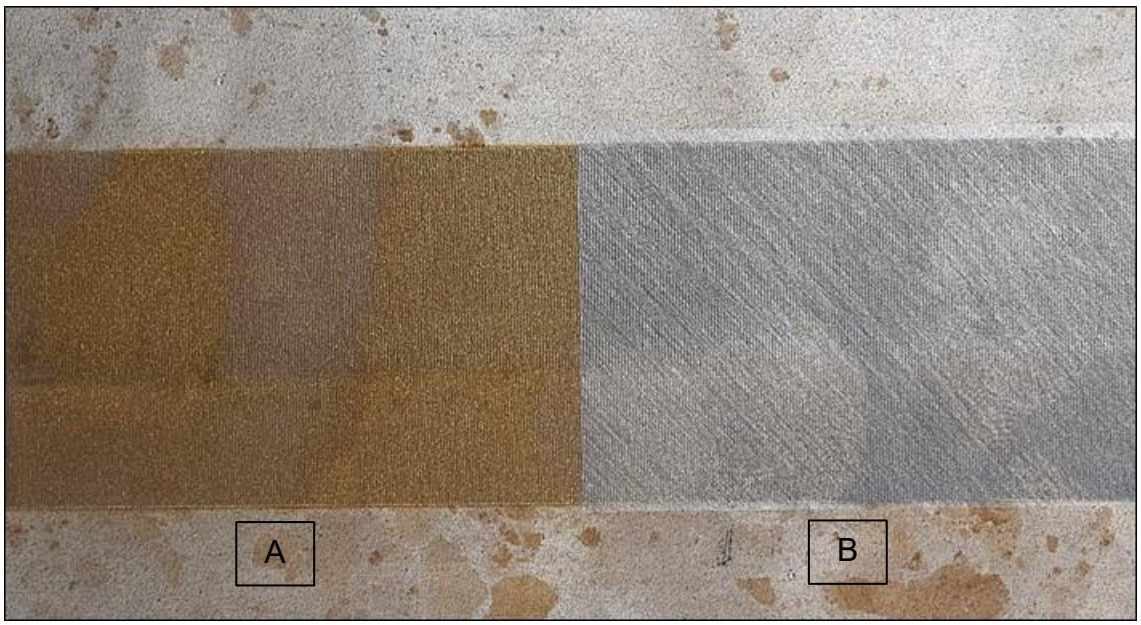

Figure 53 Sample A: 3.4 1x laser cleaning, B:3.4c 2x laser cleaning (1x 100%, 2x30%)

The topography changed when sample 3.4 was cleaned again with less “A” solvent, see in figure 54. For sample 3.4, the difference in surface height was 7.04 µm. However, the height difference of sample 3.4c, where an extra run of cleaning was performed, is now 14.76 µm, see in figure 55. This can be attributed to the fact that if the “E” is changed by exactly 180° during the second run of the cleaning, an almost flat surface could be created, leaving less chance for pitting corrosion to start, since there is not such a large height difference.

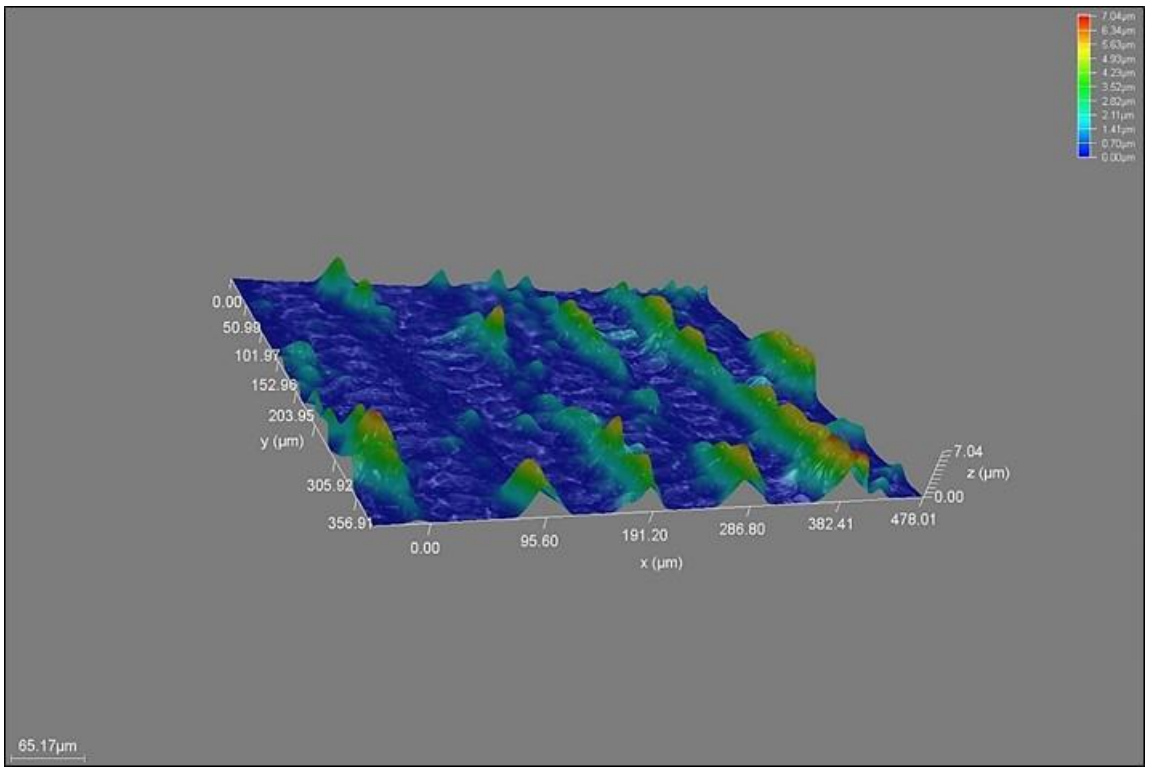

Figure 54 Surface of sample 3.4

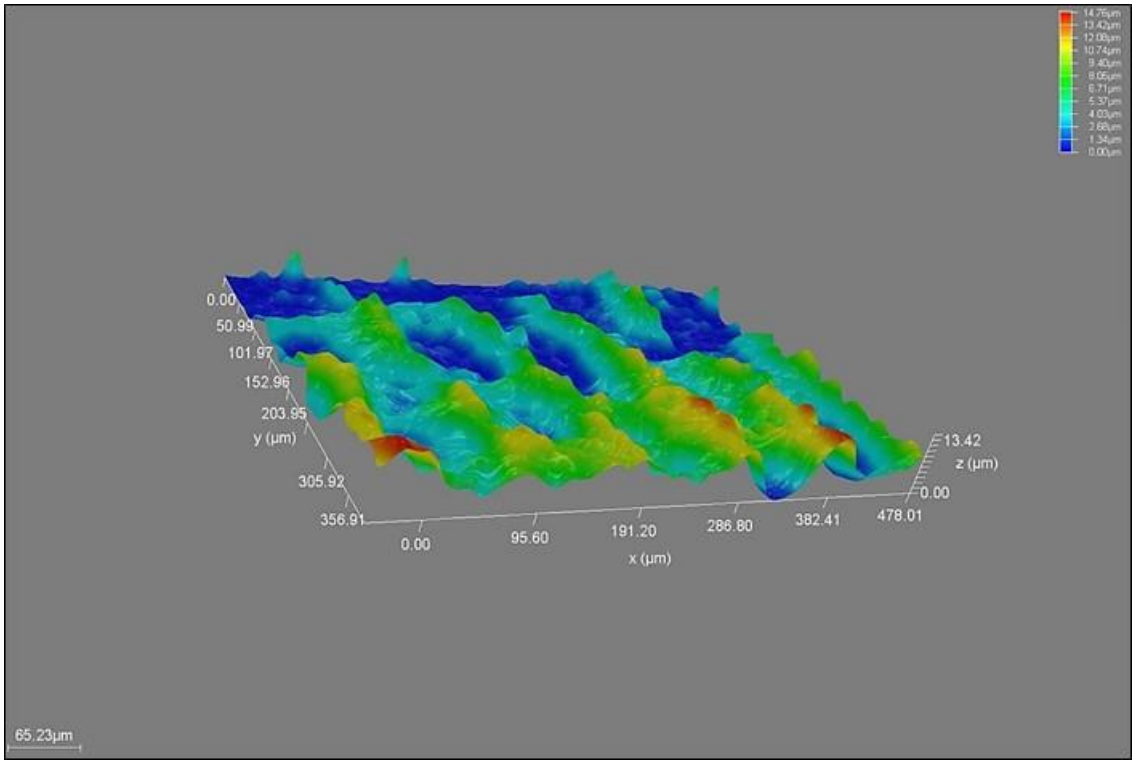

Figure 55 Surface of sample 3.4c

The results of cleaning the oxidation layer with the laser were very positive, but it is obvious that pitting occurs on the weld after cleaning. Perhaps the height of the laser could be optimised, perhaps the “E” has an important influence on the weld. However, instead of using a shielding gas for the back side, the back side can simply be cleaned with the laser. Due to this surface treatment, pitting corrosion cannot occur.

5.2.3 Corrosion potentials

As also mentioned earlier, a visually nice cleaning with the laser does not correspond to the best possible removal of the oxidation layer. Especially in the first run, this became apparent by means of the analysis "Pareto Chart of the Standardized Effects", as a visual evaluation of the samples before the salt spray test and after the salt spray test was carried out.

Measuring the corrosion potentials with the Avesta cell, the Ecorr value of the different specimens, of the material EN 1.4307, could be determined.

The evaluation of Ecorr, Erep and Epit was performed using the diagram shown in Figure 56. Thus, it was easy to see from the diagrams of the samples when pitting corrosion started and when the passivation layer could no longer be sufficiently renewed. The greater the difference between Epit and Erep, the lower the resistance to pitting corrosion. Table 22 shows the values of cyclic polarization from the paper "The effect of surface treatment AISI 316L welded joints on its corrosion behaviour in chloride solution", these samples were treated chemical or electrochemical. The following table 23 shows the corrosion potentials of the 1st run, which were laser cleaned.

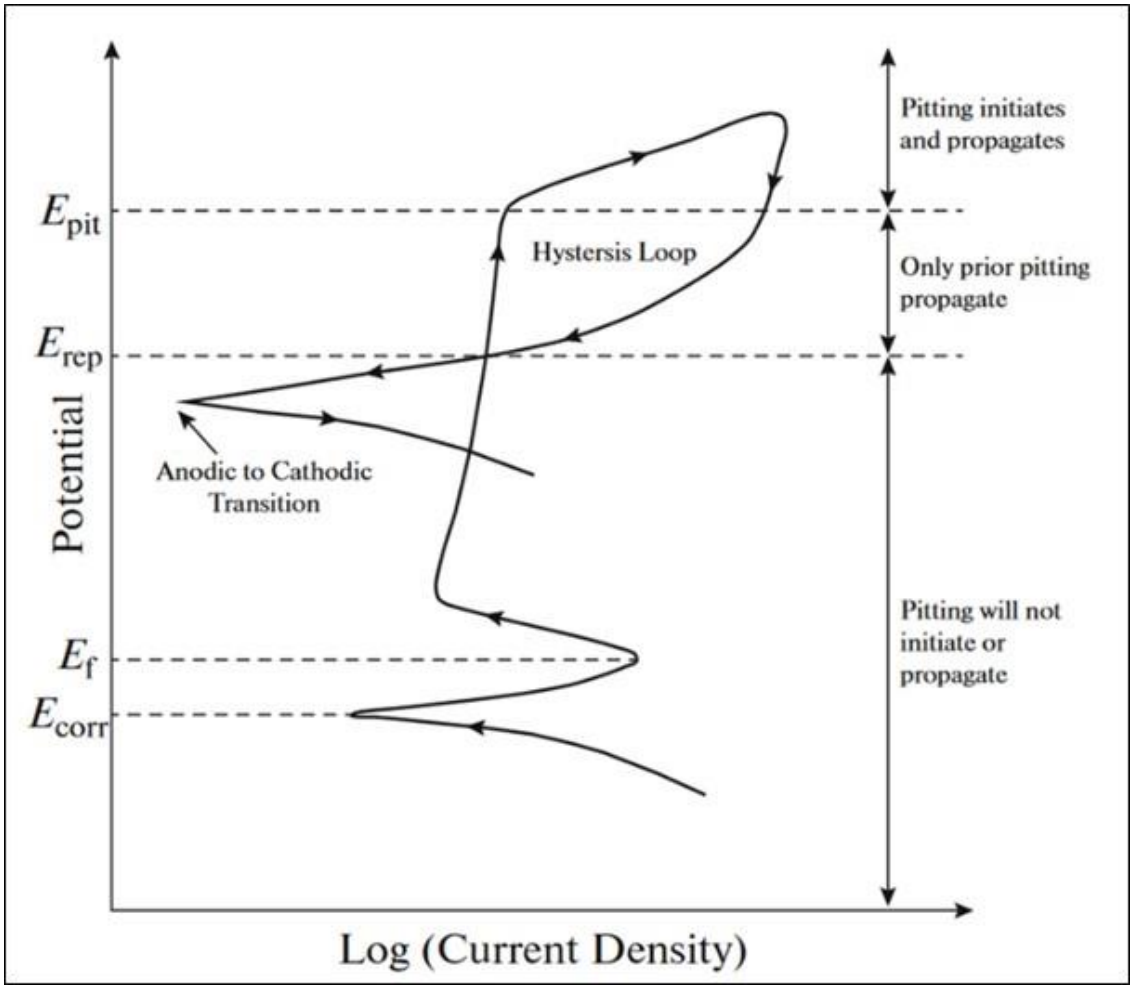

Figure 56 Pitting corrosion points. (Esmailsadeh S., Aliofkhazraei M., Sarlak H. 2018, 976-989)

An E_{rep} value could be detected in all samples from the first run, except for sample 6. In sample 6, a course without protection potential with a hysteresis loop took place. At the end, an anodic to cathodic transition takes place.

The values (E_{corr}, E_{pit}, E_{rep}) can be taken from figures 25 - 29. If E_{corr} describes the beginning of pitting corrosion, it means that if the E_{corr} point occurs earlier, this material is not as resistant to pitting corrosion as the other samples with the laser cleaning settings used. Nearly all samples (6, 9, 16 and ref) show a low risk for the material in terms of corrosion rate, only sample 3 from the first run shows moderate risk, which means that the material is not corrosion proof, but useful in certain cases.

However, it should be noted that one of the cable connections was damaged during the analysis. Therefore, these results and the analysis of the other samples with the Avesta cell cannot be used to draw the conclusion of this bachelor thesis, as these values cannot make a representative statement. Since in paper "The effect of surface treatment AISI 316L welded joints on its corrosion behaviour in chloride solution" written by Vrsalovic et. al., especially the E_{corr} values are in the range of -0.273 up to -0.370, if the weld is cleaned with the laser, the values cannot be so extremely good.

Since in the paper the surface was cleaned in four different ways. As also shown in the table 22:

- Sample A: ultrasonic cleaning in ethanol and rinsing with deionized water.
- Sample B: Ultrasonic cleaning in ethanol, chemical pickling in pickling solution (10 % HNO_3 + 10 % HF + 10 % H_2O_2) for 40 minutes and rinsing with deionized water.
- Sample C: Ultrasonic cleaning in ethanol, chemical pickling in pickling solution (10 % HNO_3+ 10 % HF + 10 % H_2O_2) for 40 min, passivation in 25 % nitric acid solution for 30 min and rinsing with deionized water.
- Sample D: mechanical grinding with different SiC paper up to a grain size of 1000, polishing with polishing suspensions, ultrasonic cleaning in ethanol, chemical pickling in pickling solution (10 % HNO_3 + 10 % HF + 10 % H_2O_2) for 40 min, passivation in 25 % Ni-solution for 30 min and rinsing with deionized water. (Vrsalovic L. et al. 2023, 168-173)

Table 22 Cyclic Polarization results of the paper "The effect of surface treatment AISI 316L welded joints on its corrosion behaviour in chloride solution" (Vrsalovic L. et al. 2023, 168-173)

Sample	i_{corr} (μA cm^{-2})	E_{corr} (V)	E_p (V)	(E_p – E_{corr}) (V)
A	0.73	–0.273	–0.007	0.266
B	0.54	–0.370	0.193	0.563
C	0.42	–0.295	0.345	0.640
D	0.38	–0.345	0.475	0.820

Also, in another paper "influence of surface treatment on corrosion resistance of Cr-Ni steel" written by Brajlovi et. al. where the material was 304L, almost the same material used for the bachelor thesis, the E_{corr} range was between -100 mv to -250 mV.

The samples were treated in two different ways: chemical and electrochemical heat tint cleaning with "classical" and "environmentally friendly" solutions. (Brajkovi T, Juraga I., Šimunovic V. 2013, 131-133)

It is almost impossible for the samples from the Bachelor thesis to have such an extremely positive effect on the pitting resistance due to the lesion cleaning. Comparing the values of the first run, see in the table 23, with those of the two papers, it is clear to see that the values of the bachelor thesis cannot correspond to reality. However, if the values would be correct, it can be determined from the table 24, that the CR value is so low that the material is "corrosion proof". Only in the case of sample three, the laser setting would not be sufficient for cleaning the oxidation layer, so the use for sample three is "the material is not corrosion proof, but useful in certain cases".

Table 23 Pitting corrosion points of the 1st run

Type	i_{corr}(µA/cm²)	E (g)	ρ(g/m³)	CR (Corrosion rate (mm/y))	E_{corr} (V)	i_{corr} (µA/cm²)
3	1.22	238.40	7.80	0.12	-0.15	1.22
6	0.31	237.30	7.80	0.03	-0.05	0.31
9	0.55	233.60	7.80	0.05	-0.09	0.55
16	0.22	224.50	7.80	0.02	-0.03	0.22
Ref	0.24	320.10	7.80	0.03	-0.23	0.24

Table 24 Classification of uniform corrosion rates:

Risk	Corrosion rate [mm/year]	Corrosion symbol	Interpretation
Low	<0.1	Green	The material is corrosion proof.
Moderate	0.1-1	Yellow	The material is not corrosion proof, but useful in certain cases.
Severe	>1	orange	Serious corrosion. The material is not usable.

6 CONCLUSIONS

6.1 Welding properties of the various types of microstructures

Using the chromium equivalent and nickel equivalent calculations shown below, it was possible to calculate the output for the 3rd test run, see table 25. With the laser cleaning of the reverse side of these results, which can also be seen in Figure 4, for the material 304. Thus, with the settings used for the 3rd run, the purging gas can be replaced with a laser cleaning with good conscience.

- Chromium equivalent = %Cr+1,5*Si%+%Mo
- Nickel equivalent =%Ni+30*(%C+%N) + 0,5*(%Mn+%Cu+%Co)

Table 25 Chromium- and Nickel equivalent

Sample	Chromium equivalent [%]	Nickle equivalent [%]	Cr/Ni
1	19.96	7.78	2.57
2	19.53	8.36	2.34
7	19.98	8.4	2.38
Ref	18.18	6.715	2.71

6.2 EDS-analysis

When evaluating the elements, it is important to pay attention to the proportion of O, Cr, Ni and Fe. The higher the O content, the thicker the oxidation layer and the easier it is for pitting to occur. If, on the other hand, the Cr and Ni content is higher, the sample is more resistant to corrosion.

Depending on the setting, the percentage of elements in the samples varies; especially in the last sample (the 3rd run), the chromium content after cleaning was over 19 %, which is very high for the material (EN 1.4307).

It should also be noted that the Mn content in all the "cleaned" samples is extremely low compared to the reference material, but the content is still very high for this type of material. Manganese is normally used in small amounts to deoxidise molten steel. Therefore, it could be that welding directly at the weld results in a higher Mn content. The most important point, that the O% content decreases, could clearly be achieved in the 3rd pass with laser cleaning.

6.3 Pitting corrosion resistance

Also, in the second run, the pitting corrosion of the specimens, as seen in figure 41, was much lower than the results of the paper "Influence of surface treatment on the corrosion resistance of Cr-Ni steel", but these specimens were immersed only 24 h in the $FeCl_3$ solution, and still the test results showed much more pitting corrosion than the specimens with the laser cleaning of the oxidation layer. As mentioned before, these samples have even been treated chemically or electrochemically and still pitting corrosion could be formed at the oxidation layer, see figure 57 and figure 58. However, it was not possible to find out whether pitting occurred at the weld seam, as the laser cleaned samples showed pitting

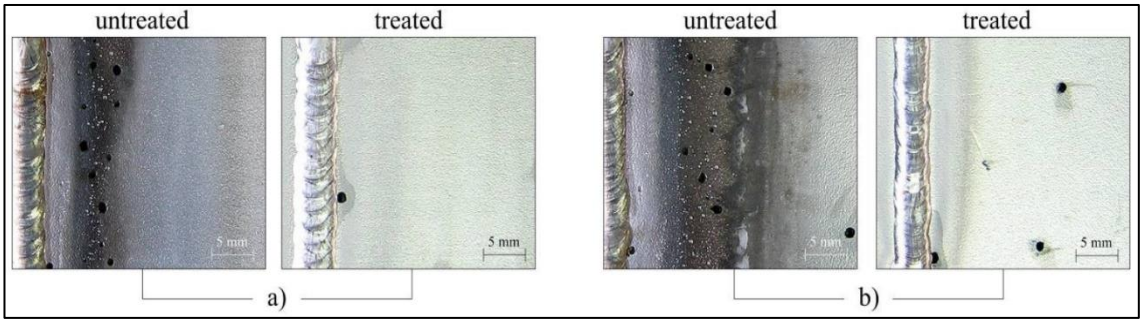

Figure 57 After $FeCl_3$- treatment for 24h, samples: chemical surface treatment: a) “classical solution”, b) environmentally friendlier” (Brajkovi T., Juraga I., Šimunovic V. 2013, 131-133)

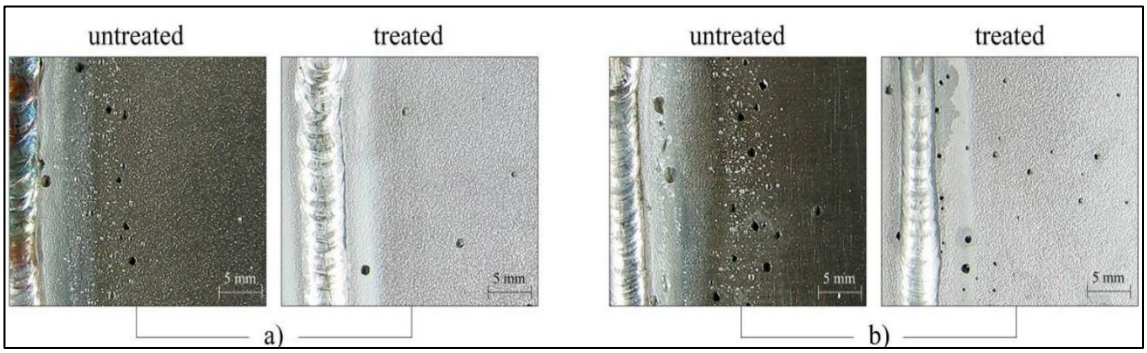

there.

Figure 58 After $FeCl_3$- treatment for 24h, samples: electrochemical surface treatment: a) “classical solution”, b) environmentally friendlier” (Brajkovi T., Juraga I., Šimunovic V. 2013, 131-133)

In the case of the 3.run, laser cleaning with these settings will cause the surface to form an oxidation layer due to the high temperatures previously reached during welding. It should be noted that the range of values that varies for the samples is very small, so it does not matter which settings of 3.run are used.

After the sample was immersed in the FeCl3 solution for three days, moderate to severe pitting corrosion occurred on the root side outside the laser cleaning area, see figure 61. Thus, although no oxidation occurred in this area, no oxidation layer is present there. Therefore, it can be assumed that laser cleaning of the surface is an important precautionary measure to prevent pitting corrosion in stainless steel.

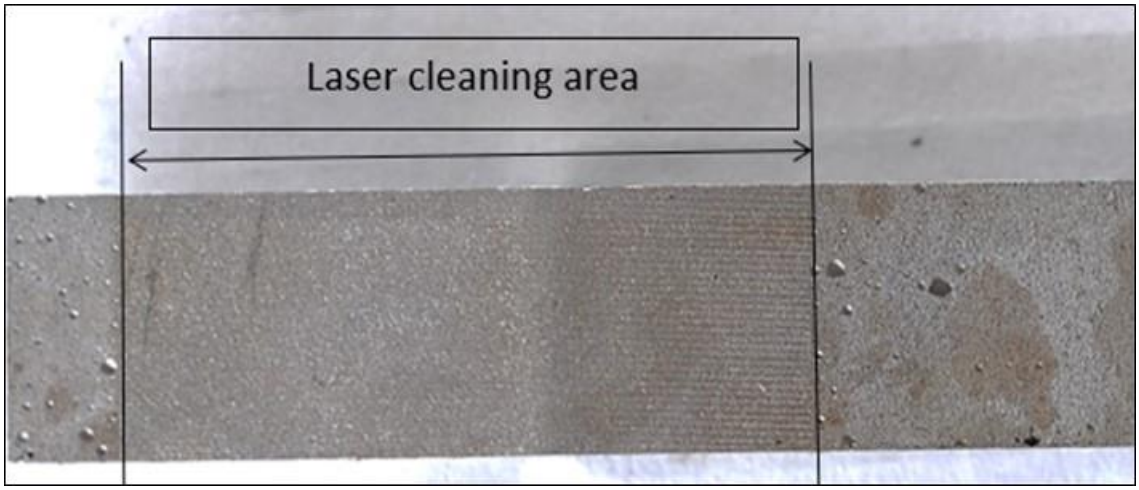

Figure 59 Root side of the sample 3.4c

6.4 Importance of laser cleaning

According to all the results, it can be confirmed with a clear conscience that laser cleaning, which removes the oxidation produced during welding, is a good, if not the better alternative for austenitic stainless steel than traditional mechanical or chemical cleaning in combination with pickling and passivation cleaning. In addition, the laser cleaning setting can be easily and precisely adapted to the sample. This in turn affects the time required, so laser cleaning has great potential to be used as an automatic component in production facilities worldwide as a cleaning tool. Furthermore, laser cleaning offers an environmentally friendly alternative since no chemical solvents are required. As with mechanical cleaning by pickling, laser cleaning does not cause wear and tear of the equipment or contamination, but only a very small amount of dust, which can be avoided with the right settings. Experiments showed that corrosion could be avoided also in the root side as well even when tested according to the G48-11 standard, while no shielding gas was used during welding. Root side laser cleaning of the specimen restored the corrosion resistance. For these reasons, basically laser cleaning is an extremely environmentally friendly and long-term cost-effective method for removing oxide layer from stainless steel welds to ensure corrosion resistance in welded structures.

REFERENCES

Brajkovi T, Juraga I.,Šimunovic V. 2013 Influence of surface treatment on corrosion resistance of Cr-Ni Steel [Online], Zagreb, 131–133. Available at https://hrcak.srce.hr/file/153148 (Accessed 13 March 2023).

Brenner A. 2021 Sequentielle Ultrakurzpuls-Laserbearbeitung zur effizienten Oberflächentexturierung: Ergebnisse aus der Lasertechnik (Dissertation) [Online], 25–29. Available at https://publications.rwth-aachen.de/record/822218/ (Accessed 19 March 2023).

Esmailsadeh S., Aliofkhazraei M., Sarlak H. 2018 'Interpretation of Cyclic Potentiodynamic Polarization Test Results for Study of Corrosion Behavior of Metals: A Review', Protection of Metals and Physical Chemistry of Surfaces, no. 5, 976–989 [Online]. DOI: 10.1134/S207020511805026X (Accessed 12 March 2023).

Heidelman G. 2009 Surface Cleaning with Laser Technology [Online], 38–41. Available at https://www.nmfrc.org/pdf/psf2009/2009-11-38.pdf (Accessed 12 March 2023).

Hügel H., G. T. 2009 Laser in der Fertigung: Strahlquellen, Systeme, Fertigungsverfahren [Online], 2nd edn, Wiesbaden, Vieweg+Teubner Verlag / GWV Fachverlage GmbH Wiesbaden, 13–14. Available at https://www.scirp.org/(S(lz5mqp453edsnp55rrgjct55))/reference/ReferencesPapers.aspx?ReferenceID=1758264 (Accessed 19 March 2023).

Informationsstelle Edelstahl Rostfrei 2023 Einfluß wichtiger Legierungs- und Spurenelemente auf die Werkstoffeigenschaften [Online]. Available at https://www.edelstahl-rostfrei.de/werkstoff/werkstoffdaten/chemische-bestaendigkeit-nichtrostender-staehle-1 (Accessed 20 March 2023).

Jinghua H.,Xudong C.,Sha W.,Guoying F, Guoliang D., Ruifeng H. 2017 Laser effects based optimal laser parameter identifications for paint removal from metal substrate at 1064 nm: a multi-pulse model [Online], Taylor & Francis, Journal of Modern Optics, vol. 64, no. 19, 1947–1955. Available at https://www.tandfonline.com/doi/abs/10.1080/09500340.2017.1330433 (Accessed 12 March 2023).

Kämmerer B. 2012 Abhängigkeit der Korrosionsbeständigkeit von der chemischen Oberflächenzusammensetzung von Chromstählen (Dissertation zur Erlangung des Doktorgrades der Mathematisch- Naturwissenschaftlichen Fakultät der Universität Augsburg) [Online], Augsburg, 17–26. Available at https://d-nb.info/1077702299/34 (Accessed 12 March 2023).

Katsich C. 2010 Hochtemperatur-Werkstoffverhalten von Eisen-Basislegierungen bei Kombination von Schlag und Abrasion (Diplomarbeit) [Online], Leoben, 20–21. Available at https://pureadmin.unileoben.ac.at/ws/portalfiles/portal/2204981/AC08459622n01vt.pdf (Accessed 12 March 2023).

Laren M. 2004 ‘Avesta Welding: The Avesta Welding manual practice and products for stainless steel welding’, 95–100 [Online]. Available at http://www.steel-stainless.org/media/1558/avesta-welding-handbook.pdf (Accessed 11 March 2023).

Laserax 2020 How Does Laser Cleaning Work in 5 Steps [Online]. Available at https://www.laserax.com/blog/how-does-laser-cleaning-work (Accessed 19 March 2023).

Lee D., C. M. 2006 ‘Particle generation by ultraviolet-laser ablation during surface decontamination’, Journal of the Air & Waste Management Association, no. 11, 1591–1596 [Online]. DOI: 10.1080/10473289.2006.10464555 (Accessed 15 March 2023).

Leffler B. 2013 Stainless: stainless steels and their properties [Online], 4–9. Available at https://www.tf.uni-kiel.de/matwis/amat/iss/kap_9/articles/stainless_steel.pdf (Accessed 10 March 2023).

Outokumpo 2023 Stainless steels for corrosive environments: Outokumpu Core range datasheet [Online], 1.4307. Available at https://www.outokumpu.com/en/products/product-ranges/core (Accessed 11 March 2023).

Qiumei B.,Yu X., Baozhen Z., Zenghu C., Shuting L. 2013 Femtosecond laser ablation of indium tin-oxide narrow grooves for thin film solar cells [Online], Optics & Laser Technology, vol. 45, 395–398. Available at https://www.sciencedirect.com/science/article/pii/S0030399212002861 (Accessed 19 March 2023).

Razab et al. 2018 ‘A review of incorporating Nd:YAG laser cleaning principal in automotive industry’, Journal of Radiation Research and Applied Sciences, [Online] no. 4, 393–402. Available at https://www.sciencedirect.com/science/article/pii/S168785071830089X (Accessed 19 March 2023)

Simms H. 2011 Oxidation behaviour of austentic stainless at high temperature in supercritical plant (Master of research) [Online], The University of Birmingham, 6–7. Available at https://core.ac.uk/download/pdf/1631537.pdf (Accessed 11 March 2023).

Simon D. 2019 Hochtemperaturoxidationsstudien zum Wasserdampfeinfluss auf thermisch wachsende Chromoxidschichten: Effect of water vapour on high-temperature corrosion on thermally grown chromia scales (Dissertation) [Online], Siegen. Available at https://dspace.ub.uni-siegen.de/handle/ubsi/1552?locale=en (Accessed 12 March 2023).

Singh A. 2020 Nanoparticle Synthesis by Pulsed Laser Ablation: From H20 to pressurized Co2: Possibilities for supercritical fluid as reactive environment (Dissertations) [Online], Tampere University, 27–28. Available at https://trepo.tuni.fi/handle/10024/122935?show=full (Accessed 19 March 2023).

Suter T. A. 1997 Mikroelektronische Untersuchungen bei austentitischen "rostfreien" Stählen: Messtechnik- Lochinitiierung- Mikroelektochemie an Schweissnähten (Doctoral Thesis) [Online], Zürich, 123–132. Available at https://www.google.com/search?client=firefox-b-d&q=Suter%2C+T.+A.%2C+1997%2C+Mikroelektronische+Untersuchungen+bei+austenitischen+%22rostfreien%22+St%C3%A4hlen%3A+Messtechnik+-+Lochinitiierung+-+Mikroelektrochemie+an+Schweissn%C3%A4hten.+ETH+Zurich (Accessed 11 March 2023).

Teneva-Kosseva G. 2005 Oxidschichtbildung und Materialprobleme metallischer Werkstoffe bei Verbrennungsprozessen mit Heizöl EL: zur Erlangung des akademischen Grades eines (Dissertation) [Online], Aachen, 3–9. Available at http://publications.rwth-aachen.de/record/60785/files/Teneva-Kosseva_Guergana.pdf (Accessed 19 March 2023).

Trydell K., Holgersson. J. 2019 Pitting Corrosion Evaluation of Post-Weld Cleaning Methods for Stainless Steel Welds (Research report) [Online], Stockholm,3, 23–24. Available at http://www.diva-portal.se/smash/get/diva2:1373405/FULLTEXT01.pdf (Accessed 19 March 2023).

Turan J. 2018 Corrosion of Austenitic Stainless Steel Welds in Chloride Containing Environments, Master Thesis in Materials Engineering, Gothenburg, Chalmers University of Technology [Online]. Available at https://odr.chalmers.se/server/api/core/bitstreams/1af0b6cb-87b4-4891-b522-ad9f79c6fa49/content (Accessed 12 March 2023).

Vrsalovic L. et al. 2023 The effect of surface treatment AISI 316L welded joints on its corrosion behaviour in chloride solution [Online], Bratislava, 168–171. Available at https://www.researchgate.net/publication/304065042_The_effect_of_surface_treatment_AISI_316L_welded_joints_on_its_corrosion_behaviour_in_chloride_solution (Accessed 19 April 2023).

Westin E. M. ,Olsson C.-O.A, Hertzman, S. 2008 ‘Weld oxide formation on lean duplex stainless steel’, Corrosion Science, vol. 50, no. 9, 2620–2634 [Online]. DOI: 10.1016/j.corsci.2008.06.024 (Accessed 19 April 2023).

Zimmermann D. 2001 Einfluss der Oberflächenorientierung und der chemischen Zusammensetzung auf das Oxidationsverhalten von β-NiAl Einkristallen (Dissertation) [Online], Stuttgart, 16–20. Available at https://elib.uni-stuttgart.de/bitstream/11682/6508/1/Diss_ges.pdf (Accessed 19 April 2023).

7 TABLE OF FIGURES

8 TABLE OF TABLES

9 APPENDICES

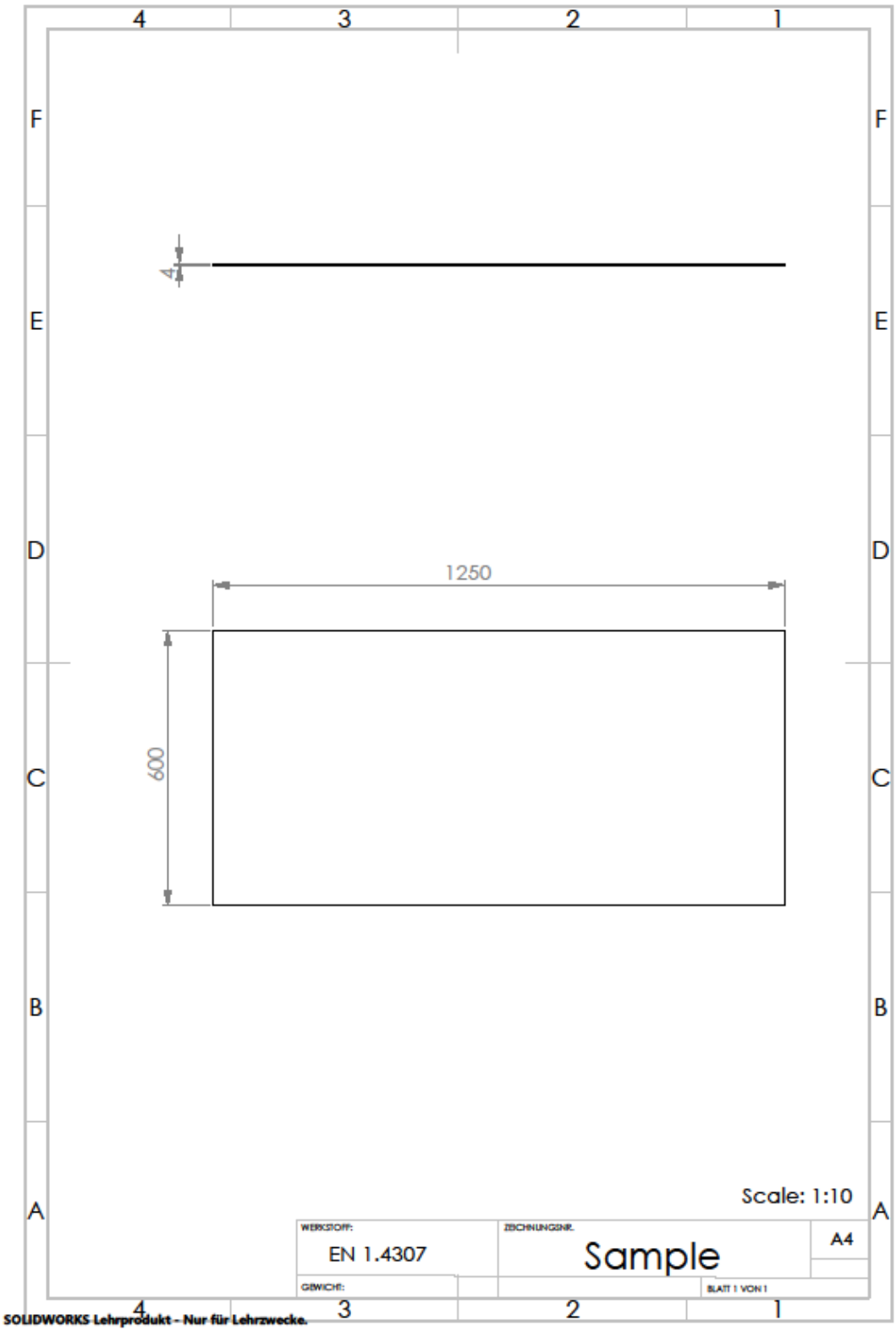

Figure 60 The size of Sample plate for the sample

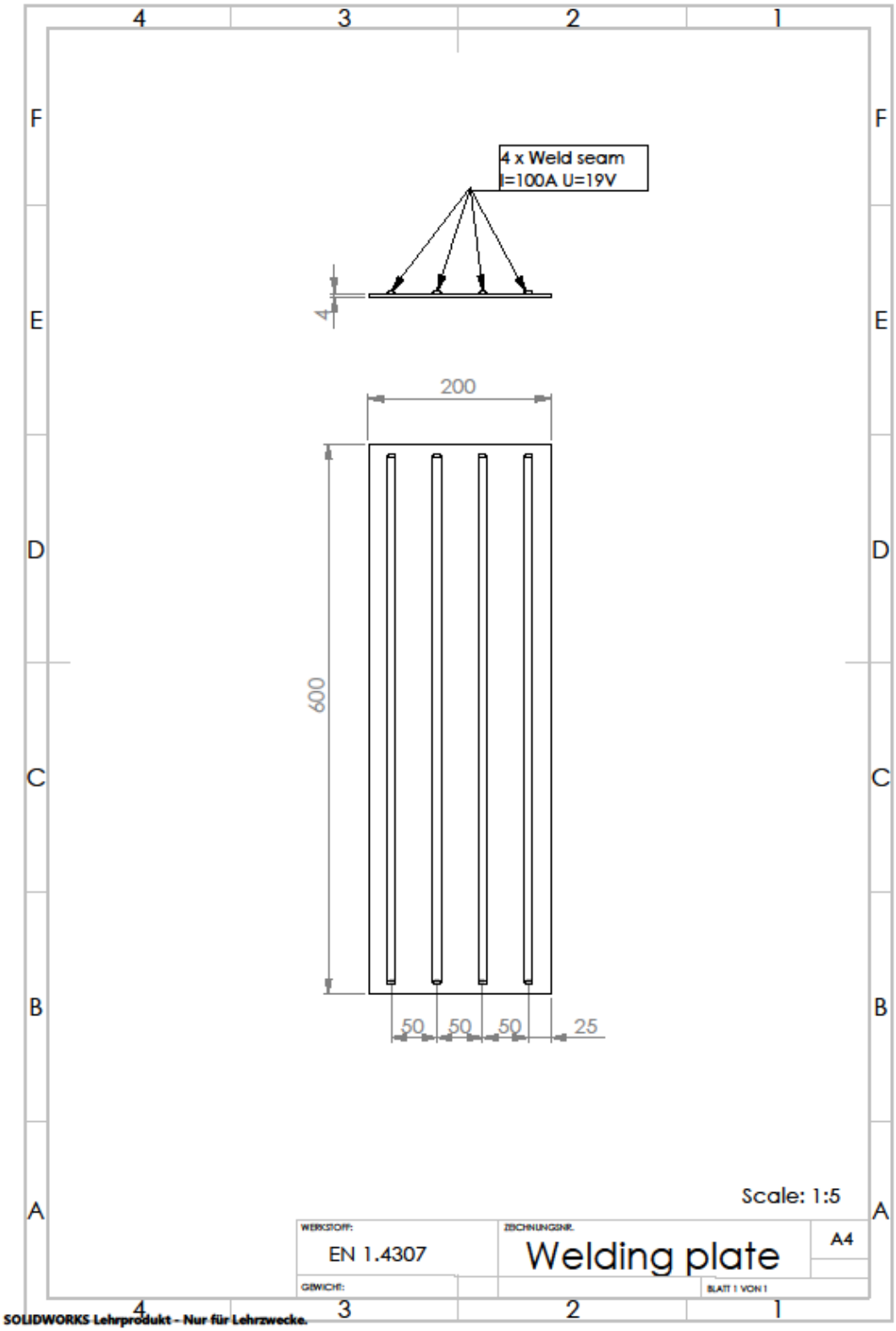

Figure 61 Sample plate with welds

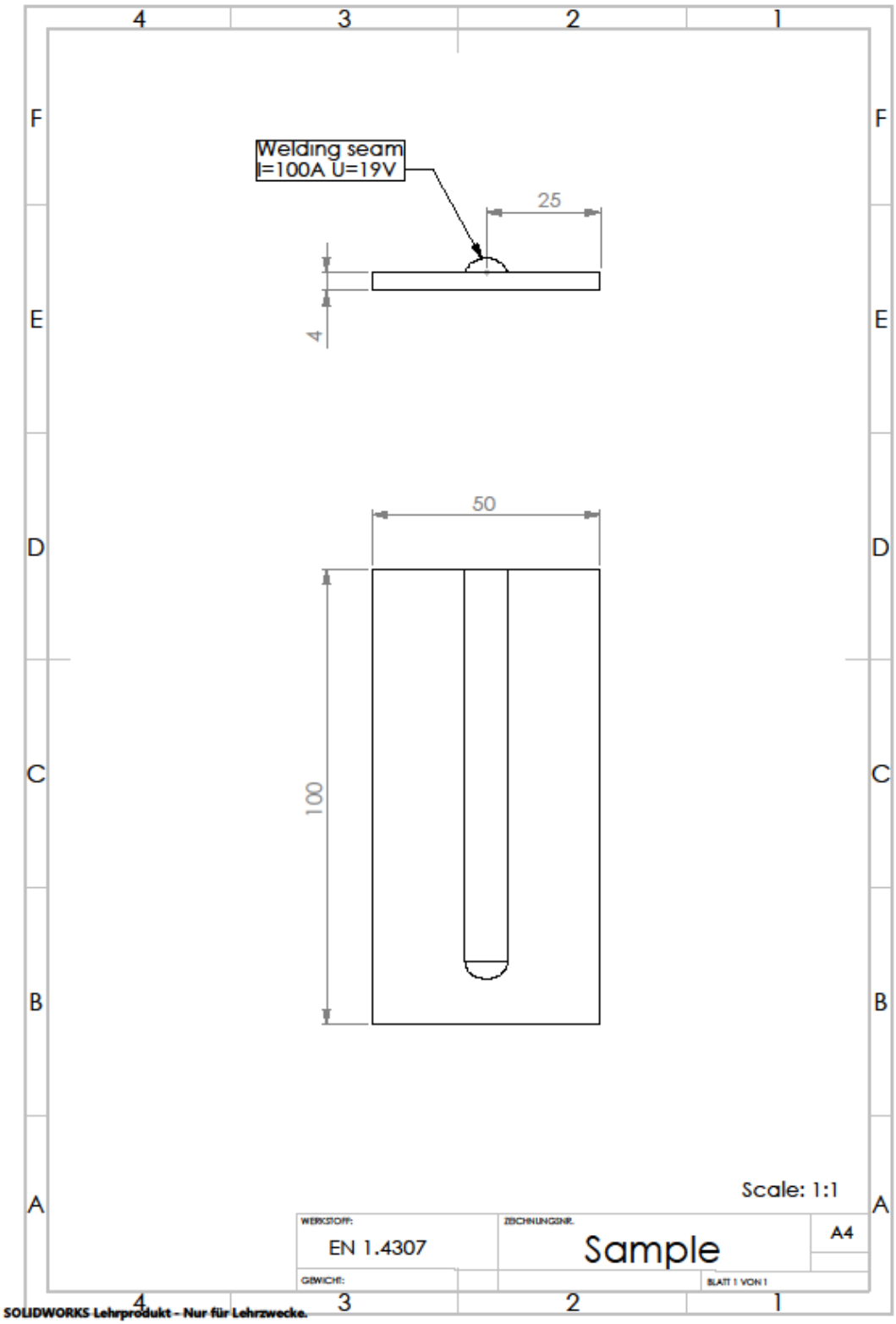

Figure 62 Sample size for the analyses

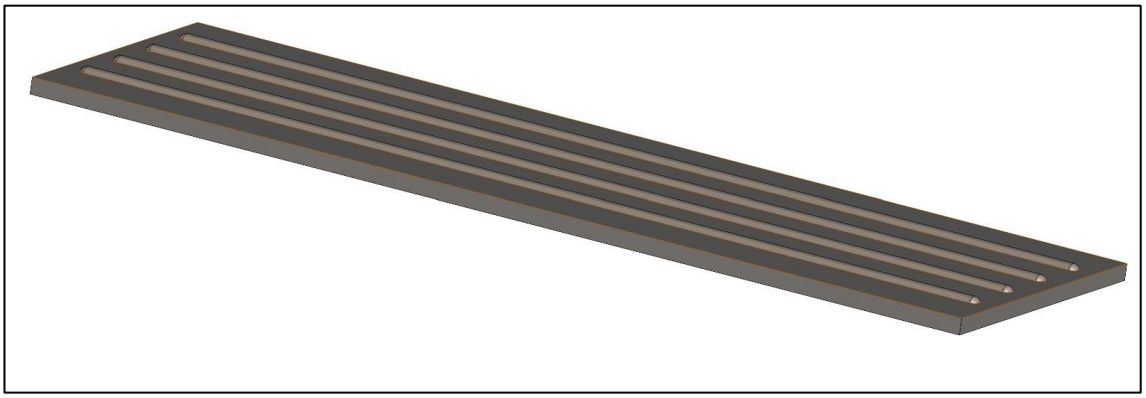

Figure 63 3D perspective of the welding plate